nature communications

Article

https://doi.org/10.1038/s41467-024-54583-6

Structural basis for Retriever-SNX17 assembly and endosomal sorting

Received: 21 March 2024

Accepted: 15 November 2024

Published online: 25 November 2024

Check for updates

Amika Singla[1,11], Daniel J. Boesch[2,11], Ho Yee Joyce Fung[3,11], Chigozie Ngoka[2], Avery S. Enriquez[2], Ran Song[4], Daniel A. Kramer[2], Yan Han[3], Esther Banarer[1], Andrew Lemoff[5], Puneet Juneja[6,10], Daniel D. Billadeau[7], Xiaochen Bai[3], Zhe Chen[3], Emre E. Turer[4] ✉, Ezra Burstein[1,8] ✉ & Baoyu Chen[2,9] ✉

During endosomal recycling, Sorting Nexin 17 (SNX17) facilitates the transport of numerous membrane cargo proteins by tethering them to the Retriever complex. Despite its importance, the mechanisms underlying this interaction have remained elusive. Here, we provide biochemical, structural, cellular, and proteomic analyses of the SNX17-Retriever interaction. Our data reveal that SNX17 adopts an autoinhibited conformation in the basal state, with its FERM domain sequestering its C-terminal tail. The binding of cargo proteins to the FERM domain displaces the C-terminal tail through direct competition. The released tail engages with Retriever by binding to a highly conserved interface between its VPS35L and VPS26C subunits, as revealed by cryogenic electron microscopy (cryo-EM). Disrupting this interface impairs the Retriever-SNX17 interaction, subsequently affecting the recycling of SNX17-dependent cargoes and altering the composition of the plasma membrane proteome. Intriguingly, the SNX17-binding pocket on Retriever can be utilized by other ligands containing a consensus acidic C-terminal tail motif. Together, our findings uncover a mechanism underlying endosomal trafficking of critical cargo proteins and reveal how Retriever can potentially engage with other regulatory factors or be exploited by pathogens.

Plasma membrane (PM) proteins undergo frequent internalization into the endosomal compartment, where they are either routed back to the cell surface for reuse or to lysosomes for degradation. The maintenance of this trafficking process is vital for cellular homeostasis and involves intricate regulatory systems. Among these, the trimeric protein complex Retriever plays a crucial role in identifying PM proteins, also called cargoes, for recycling from endosomes. Composed of VPS35L, VPS26C, and VPS29 (Fig. 1a), Retriever is remotely related to

[1]Department of Internal Medicine, University of Texas Southwestern Medical Center, 5323 Harry Hines Boulevard, Dallas, TX 75390, USA. [2]Roy J. Carver Department of Biochemistry, Biophysics & Molecular Biology, Iowa State University, 2437 Pammel Drive, Ames, IA 50011, USA. [3]Department of Biophysics, University of Texas Southwestern Medical Center, 6001 Forest Park Road, Dallas, TX 75390, USA. [4]Center for the Genetics of Host Defense, University of Texas Southwestern Medical Center, 5323 Harry Hines Boulevard, Dallas, TX 75390, USA. [5]Department of Biochemistry, University of Texas Southwestern Medical Center, 5323 Harry Hines Boulevard, Dallas, TX 75230, USA. [6]Cryo-EM facility, Office of Biotechnology, Iowa State University, 2437 Pammel Drive, Ames, IA 50011, USA. [7]Division of Oncology Research, College of Medicine, Mayo Clinic, Rochester, MN 55905, USA. [8]Department of Molecular Biology, University of Texas Southwestern Medical Center, 5323 Harry Hines Boulevard, Dallas, TX 75390, USA. [9]On sabbatical leave at Department of Biophysics, University of Texas Southwestern Medical Center, 6001 Forest Park Road, Dallas, TX 75390, USA. [10]Present address: Thermo Fisher Scientific, 5350 NE Dawson Creek Drive, Hillsboro, OR 97124, USA. [11]These authors contributed equally: Amika Singla, Daniel J. Boesch, Ho Yee Joyce Fung.
✉e-mail: Emre.Turer@UTSouthwestern.edu; Ezra.Burstein@UTSouthwestern.edu; Stone@iastate.edu

https://doi.org/10.1038/s41467-024-54583-6

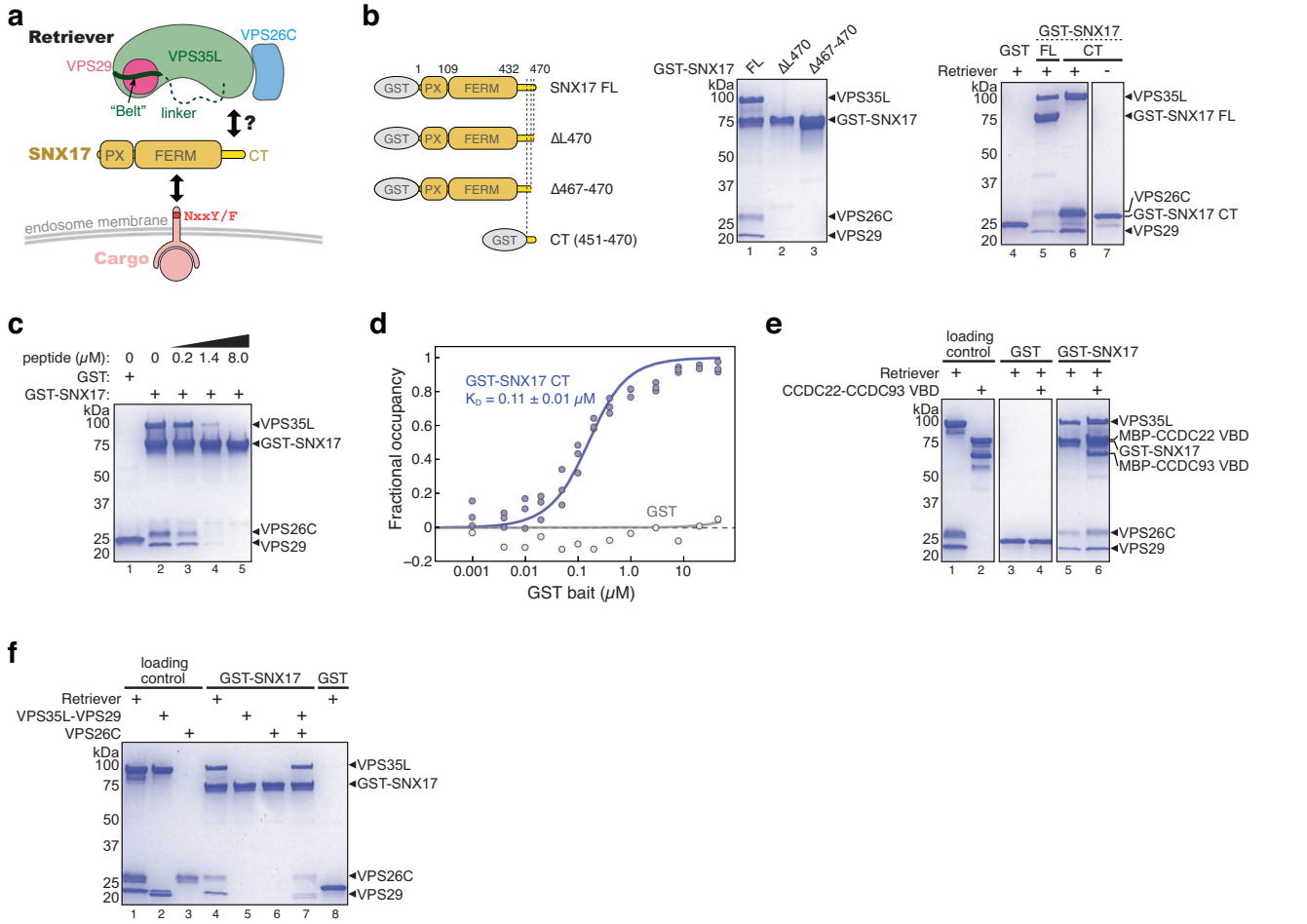

Fig. 1 | SNX17 uses its C-terminal tail to bind Retriever. a Cartoon depiction of Retriever and the domain architecture of SNX17. **b** Cartoon representation of GST-SNX17 constructs used (left panel) and Coomassie blue-stained SDS PAGE gels showing in vitro GST pull-down between indicated GST-SNX17 constructs and Retriever (right panel). **c** Coomassie blue-stained SDS PAGE gels showing in vitro GST pull-down between GST-SNX17 and Retriever in the presence of increasing concentrations of a competing peptide consisting of the last 20 amino acids of SNX17. **d** Binding isotherms obtained from EPD assays measuring the binding affinity between GST-SNX17 CT and Retriever. Data were pooled from three independent experiments and globally fitted to a one-binding site model to obtain the K_D and fitting error[48]. GST pull-down as a negative control was from one experiment. Representative Coomassie blue-stained SDS-PAGE gels from the EPD experiments are shown in Supplementary Fig. 1a. Coomassie blue-stained SDS PAGE gels showing in vitro GST pull-down between GST-SNX17, and Retriever complexed with CCDC22-CCDC93 VBD dimer (**e**) or isolated subunits of Retriever (**f**). Representative results from at least two independent experiments are shown for each pull-down. Source data for **b**–**f** are provided as a Source Data file.

the well-studied endosomal recycling complex Retromer[1–3], which handles a separate subset of cargoes. Recent studies have revealed that while Retriever shares a similar overall architecture with Retromer, it possesses distinct structural features and regulatory mechanisms[4–7].

Retriever manages the recycling of a broad spectrum of cargoes, including integrins, tyrosine receptor kinases, G-protein coupled receptors (GPCRs), and lipoprotein receptors[4,8,9]. In contrast, Retromer handles a distinct subset of cargoes, such as various transporters (DMT1, ATP7A/B, GLUT1), GPCRs (β2AR), and SorL1 (a sorting factor implicated in Alzheimer's disease)[10–15]. Both Retriever and Retromer cooperate with additional factors to ensure efficient cargo sorting. Integral to the function of both complexes is the WASH regulatory complex, which promotes Arp2/3-mediated actin polymerization at endosomal membranes[16–19]. In addition, Retriever associates with the COMMD/CCDC22/CCDC93 complex (CCC)[8] to form a larger structure called the Commander assembly[20–22]. In this assembly, the ten COMMD proteins form a ring-like structure[5–7], while the CCDC22-CCDC93 dimer connects this ring to Retriever using different domains. The dimer also interacts with DENND10, a putative Rab guanine nucleotide exchange factor (GEF) whose functions are not yet clearly defined.

Sorting nexin proteins represent crucial regulatory factors responsible for tethering Retromer or Retriever to endosomal membranes and their specific cargoes[23]. Categorized into seven groups based on their domain organization, sorting nexins participate in many facets of protein trafficking within cells[23]. Retromer-associated sorting nexins, such as the PX domain-only SNX3[24] and the BAR domain-containing SNX1, SNX2, SNX5, and SNX6[25], mediate membrane deformation. Among these, some sorting nexins like SNX3, SNX5, and SNX6[26–28] also contribute to cargo recognition. Another important sorting nexin, SNX27, which contains both PDZ and FERM domains, serves to tether Retromer to over 100 specific cargoes[10,15]. SNX27 accomplishes this by binding to the VPS26 subunit of Retromer and, through its PDZ domain, connecting Retromer to PDZ binding motifs in the cytoplasmic tails of these cargoes[29]. In contrast, SNX17, a distant homolog of SNX27 that also contains a FERM domain, is specifically associated with Retriever. Unlike SNX27, SNX17 uses its FERM domain to recognize the NxxY/F motif in the cytoplasmic tails of over 100 distinct cargo proteins[30,31]. The interaction between Retriever and SNX17 is dependent on SNX17's C-terminal tail[4], but the precise mechanism underlying their binding has yet to be deciphered (Fig. 1a).

It also remains unknown if other regulatory factors connect Retriever to additional cargoes or recycling processes.

In this study, we present the cryo-EM structure of a Retriever-SNX17 complex, along with comprehensive validation of the binding mechanism through biochemical, cellular, and proteomic analyses. Furthermore, we report the discovery of additional ligands for Retriever, which similarly interact with the complex through the conserved SNX17-binding pocket. This finding expands the repertoire of regulatory factors of Retriever and suggests versatile connections of Retriever with other potential targets.

Results

SNX17 uses its C-terminal tail to bind Retriever

Previous cellular and co-immunoprecipitation studies showed that the C-terminal (CT) unstructured tail of SNX17 is important for interacting with Retriever[4] (Fig. 1a). We first used recombinantly purified proteins to determine whether the interaction is direct. Our GST pull-down assays showed that GST-SNX17 directly interacted with Retriever and, consistent with previous cell-based results[4], the in vitro interaction relied on the C-terminal tail of SNX17 (Fig. 1b). Deleting the last four residues (Δ467-470) or the last residue (Δ470) of the tail abolished the interaction (Fig. 1b, lanes 2-3). We found that the tail was both necessary and sufficient for the interaction, as a GST-tagged tail peptide comprising the last 20 residues similarly pulled down Retriever (Fig. 1b, lane 6), and a chemically synthesized peptide of the same 20 residues of the tail could compete off the binding of GST-SNX17 in a dose-dependent manner (Fig. 1c). Using an equilibrium pull-down assay, we determined that the binding has a dissociation constant (K_D) of ~0.11 μM in our buffer condition (Fig. 1d; Supplementary Fig. 1a). In addition, in the same in vitro conditions, we found that SNX17 could similarly bind to Retriever complexed with the VPS35L binding domain (VBD) of the CCDC22-CCDC93 dimer (Fig. 1e, lane 6), the key scaffold required for CCC complex assembly[6], suggesting that SNX17 interacts similarly with Retriever alone or with the Retriever-CCC complex.

Intriguingly, SNX17 could not bind to individual subunits of Retriever, including a VPS35L-VPS29 binary subcomplex or the VPS26C subunit in isolation, and only bound to fully assembled Retriever (Fig. 1f, lanes 4-6). This is not due to misfolding or mis-assembly of the isolated components, as the interaction was readily recovered when the individually purified VPS35L-VPS29 subcomplex and VPS26C were freshly mixed in the reaction (Fig. 1f, lane 7; also see Supplementary Fig. 1b for size exclusion chromatography profiles of individual components indicating monodispersed, well-behaving materials). The above results confirm the requirement of VPS26C for binding[4] and suggest that SNX17 only directly interacts with fully assembled Retriever in vivo.

FERM domain and cargo binding regulate the CT tail of SNX17

AlphaFold structures[32] suggest that SNX17 may also engage in an intramolecular interaction between an ^{459}NFAF^{462} sequence, located −11 to −8 residues from its CT end, and the FERM domain (Fig. 2a). This interaction is similar to how NxxY/F motifs in SNX17-specific cargoes bind to the same surface of the FERM domain, as shown in previous crystal structures[30,31] (Fig. 2a, red sequences). This model suggests an intriguing regulatory mechanism where the CT tail is sequestered by binding to the FERM domain and can be displaced by cargo binding to facilitate its interaction with Retriever (Fig. 2a, right panel).

To test this model, we used individually purified CT tail and the FERM domain of SNX17 to assess their interaction and the effect of cargo peptide binding (Fig. 2b). We found that GST-CT interacted with the FERM domain as well as a longer construct containing PX-FERM, but not with full-length (FL) SNX17 (Fig. 2c, lanes 1, 2, 4). This suggests that in FL SNX17, its CT tail binds to the FERM domain, blocking it from accessing the free CT tail. The binding of GST-CT to FERM or PX-FERM was blocked by the addition of a synthetic cargo peptide from KRIT1 containing an NxxY/F motif[31] (Fig. 2a–c, lanes 3, 5), indicating that the CT tail and cargo peptide bind to the same surface on the FERM domain. We also tested whether the N-terminal PX domain binding to the headgroup of phosphoinositide 3-phosphate [PI(3)P] influences the FERM-CT interaction in SNX17 and observed no changes (Fig. 2c, lanes 4, 6), aligning with the predicted structural model showing that the PX domain and the PI(3)P binding pocket are not involved in sequestering the CT tail (Fig. 2a). We further validated the predicted structure by mutating the NxxY/F motif in the CT tail, finding that mutations in N459 and F462, but not F460, abolished the binding to the FERM domain, confirming that the sequestering relies on the NxxY/F motif in SNX17 CT (Fig. 2d).

Given the proximity of the NxxY/F motif in SNX17 to its extreme CT end, we next tested if this intramolecular interaction prevents SNX17 CT from binding to Retriever. We found that Retriever competed off the FERM domain binding to GST-CT in a dose-dependent manner (Fig. 2e, left panel). This competition is due to the CT tail binding to Retriever, as a mutant GST-CT (L470G), which is incapable of binding to Retriever, showed no impact of Retriever on its binding to the FERM domain (Fig. 2e, right panel). Conversely, the addition of the FERM domain also competed off Retriever from binding to GST-CT in a dose dependent manner (Fig. 2f, lanes 1–3). These results demonstrate that the SNX17 CT tail can only bind to either the FERM domain or Retriever, but not both simultaneously. Thus, SNX17 CT binding to FERM domain can prevent its binding to Retriever.

We then tested if cargo peptide binding to the FERM domain promotes the binding of the CT tail to Retriever. Using a pull-down condition where GST-CT shows similar levels of pull-down signals for Retriever and the FERM domain (Fig. 2f, lanes 3, 4), we added increasing concentrations of the cargo peptide and observed that the interaction between the CT tail and Retriever increased, while the interaction between the CT tail and the FERM domain decreased simultaneously (Fig. 2f, lanes 4-7). This indicates that cargo peptide binding releases the CT tail, enabling it to interact with Retriever. To further test this model with FL SNX17, we immobilized a His_6-tagged Retriever to pull down untagged FL SNX17 and observed that the addition of the cargo peptide enhanced the Retriever-SNX17 interaction (Fig. 2g, lanes 3, 4), while the addition of the short-chain PI(3)P did not have this effect (Fig. 2g, lanes 3, 5). Together, the above data suggest that SNX17 is basally autoinhibited from binding to Retriever, and cargo binding dislodges the CT tail to enhance the efficiency of SNX17 in tethering Retriever to cargo proteins (Fig. 2a, right panel).

Cryo-EM structure of Retriever bound to SNX17 CT

To understand how the CT tail of SNX17 interacts with Retriever, we next determined the structure of the Retriever-SNX17 complex using cryo-EM. After exhaustively surveying protein constructs and grid conditions, we were able to obtain a cryo-EM map with a resolution of ~3.4 Å by using Retriever mixed with saturating concentrations of the SNX17 tail peptide (Fig. 3a, Table 1, Supplementary Fig. 2). We used local refinement and local resolution-based map sharpening[33] to improve map quality and built the structural model starting with one generated by AlphaFold prediction (Fig. 3a and Supplementary Figs. 2 and 3a). The overall crescent-shaped structure of Retriever is slightly extended compared to its apo form, with an average root-mean-square deviation of ~1.9 Å (Supplementary Fig. 3b). Due to potential conformational dynamics, we could not obtain a well-resolved map for the VPS29-bound end, where the N-terminal "belt" sequence of VPS35L was found to stabilize the bound VPS29 and the CT region of VPS35L in our previous work[6] (Fig. 3a, represented by dashed line, and Supplementary Figs. 2 and 3b).

Nevertheless, the map unambiguously located the density of SNX17's CT tail over a conserved surface nestled between the VPS35L and VPS26C subunits of Retriever (Fig. 3a, b, with map quality shown in Supplementary Fig. 3c, d). This density readily accommodated 12

https://doi.org/10.1038/s41467-024-54583-6

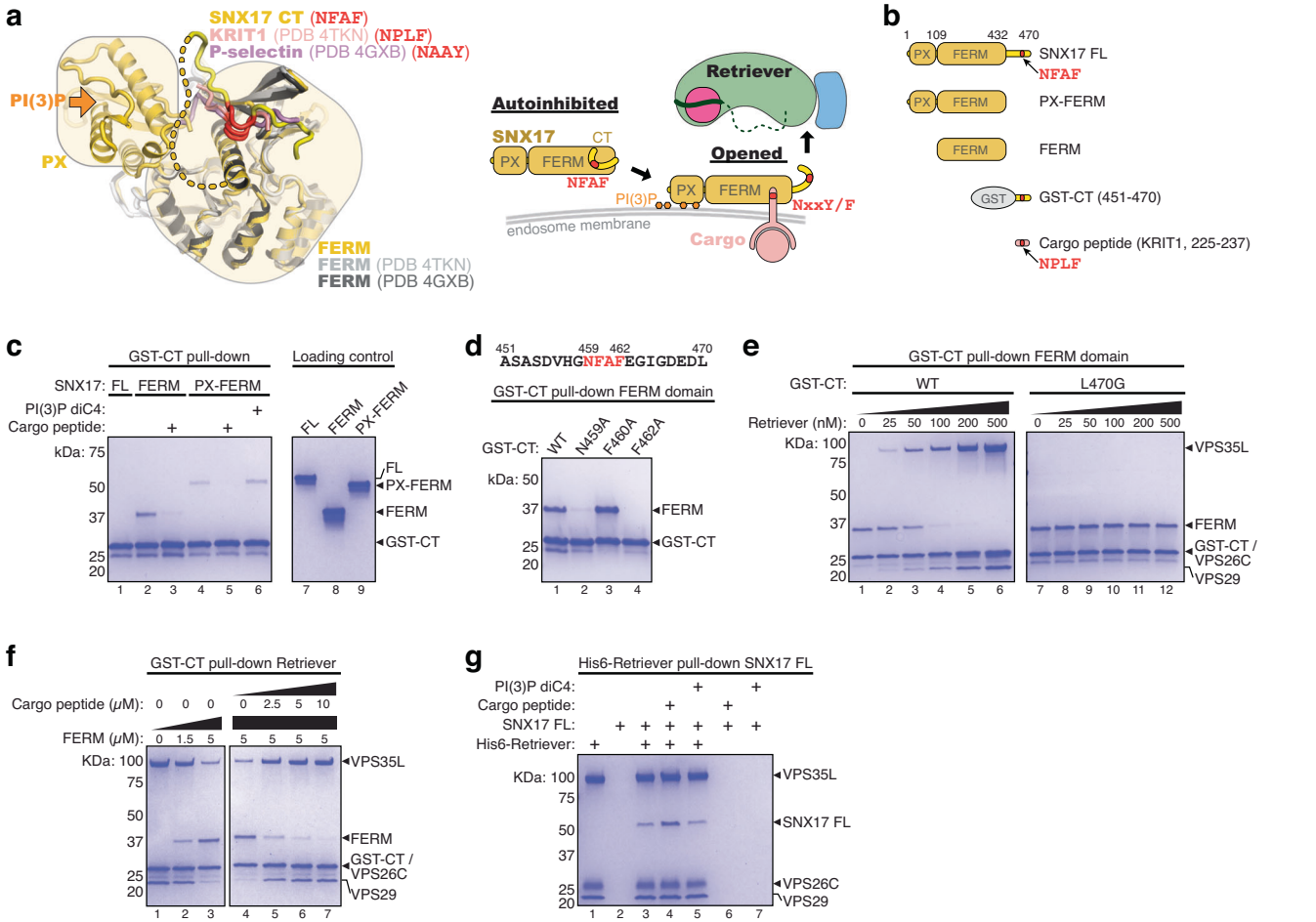

Fig. 2 | SNX17 CT tail is sequestered by FERM domain and displaced by cargo binding. a Left: Overlay of an AlphaFold model of FL SNX17 with crystal structures of the SNX17 FERM domain bound to cargo peptides. The NxxY/F motifs are highlighted in red. Right: Cartoon representation show how cargo binding displaces the sequestered CT tail to promote Retriever binding. **b** Cartoon representation of SNX17 and cargo constructs used. **c**–**g** Coomassie blue-stained SDS PAGE gels showing in vitro pull-down under the indicated conditions. **c** shows GST-SNX17 CT tail pulling down indicated SNX17 constructs in the presence of 0.6 μM KRIT1 cargo peptide or 200 μM PI(3)P diC4, a short chain, soluble PI(3)P analog. **d** shows GST-SNX17 CT tail mutants pulling down the SNX17 FERM domain. **e** shows GST-SNX17 CT tails pulling down the FERM domain in the presence of increasing concentrations of Retriever. **f** shows GST-SNX17 CT tail pulling down Retriever in the presence of FERM domain and/or increasing concentrations of cargo peptide. **g** shows His_6-tagged Retriever on TALON beads pulling down untagged FL SNX17 in the presence of 6 μM cargo peptide or 200 μM PI(3)P diC4. Representative results from at least two independent experiments are shown for each pull-down. Source data for **c**–**g** are provided as a Source Data file.

residues at the C-terminus of the peptide (Fig. 3a, b), which also encompasses the NxxF motif. The peptide adopts a uniquely twisted conformation containing two short, distorted 1-turn helices separated by a short loop (Fig. 3c, d). The majority of the interaction is mediated by a conserved and positively charged surface on VPS35L, contributed largely by residues from helices α2, α3, and α4 (Fig. 3b, c; Supplementary Fig. 4a, b). In addition, a conserved and slightly positively charged surface on VPS26C, mainly contributed by residues on Loop 1, Loop 13, and strand β12, interacts with the SNX17 peptide from the opposite side (Fig. 3c; Supplementary Fig. 4a, b). This interaction is unique to Retriever, as Retromer uses distinct surfaces to interact with adaptors, such as SNX3 and SNX27, or directly with cargoes, such as DMT1[26,29,34] (Supplementary Fig. 4c). This experimentally derived cryo-EM model of the Retriever-SNX17 complex is consistent with AlphaFold predictions, with some differences in the residues leading to the C-terminal tip of SNX17 (Supplementary Fig. 3a).

The structural model elucidates the significance of the last few amino acids of SNX17 previously shown to be critical to the binding to Retriever[4]. Remarkably, the last residue of SNX17, L470, uses both its side chain and the carboxyl group to establish a network of interactions with VPS35L critical for binding (Fig. 3c, d). Specifically, L470's carboxyl group engages with residues K204, R248, and T276 in VPS35L, while its side chain fits into a deep hydrophobic pocket formed by V205, W280, and the alkyl chains of K204 and K283 of VPS35L. These interactions explain why mutating L470 to G or deleting this residue abolished the Retriever-SNX17 interaction[4] (Fig. 1b, lane 2).

In addition to L470, the structure also explains how other residues in SNX17's tail contribute to the binding (Fig. 3c, d). At the C-terminal portion of the peptide, D469 in SNX17 is oriented towards K14 from VPS26C, while D467 in SNX17 and K204 in VPS35L engage with each other's backbone. At the N-terminal portion of the peptide, F462 in SNX17, which is part of the NxxF motif crucial for binding to the FERM domain (Fig. 2a–d), interacts with residues L208, I212, I287, and K283 in VPS35L, with the backbone of F462 and I465 in SNX17 further interacting with K283 in VPS35L. In addition, residues N459, F460, and A461 of SNX17 may form van der Waals interactions with the VPS26C surface.

It is remarkable that the sequences of both VPS35L and VPS26C that contribute to the SNX17 binding pocket, especially the residues directly involved in the interaction, are conserved across a diverse range of organisms from human to amoeba and *Arabidopsis* (Fig. 3c–e; Supplementary Fig. 4a). This suggests that the SNX17-Retriever

https://doi.org/10.1038/s41467-024-54583-6

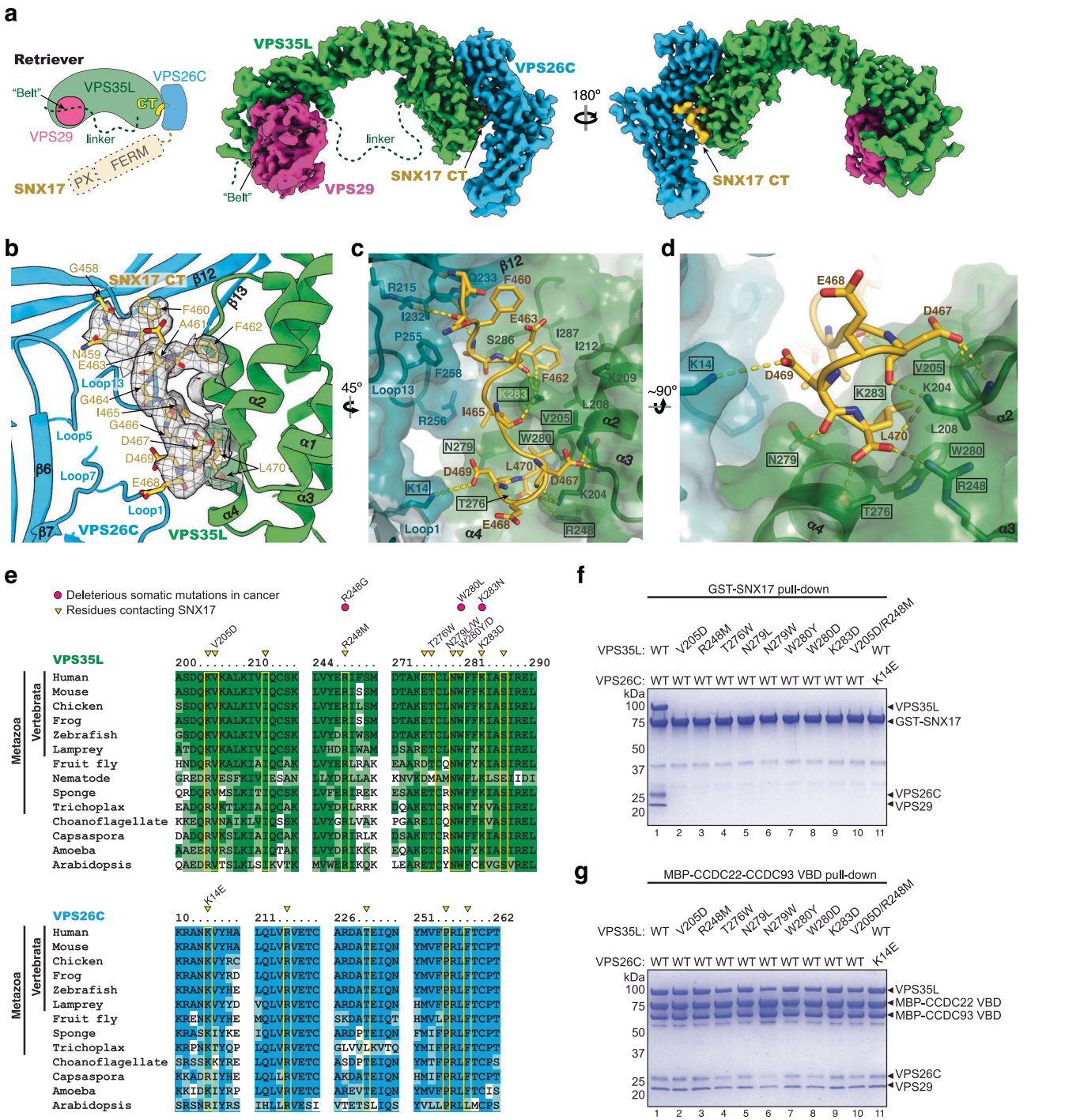

Fig. 3 | Structure of SNX17 C-terminal tail binding to Retriever. a Schematic and overall colored cryo-EM map of the SNX17 CT peptide (golden) complexed with Retriever (VPS35L in green, VPS29 in magenta, and VPS26C in cyan). Dotted lines indicate structural elements not resolved in cryo-EM. N-terminal domains of SNX17 are shown as a reference. **b**–**d** Close-up views showing key interactions between the SNX17 CT peptide (carbon in green, oxygen in red, and nitrogen in blue) and its binding surface on VPS35L and VPS26C: **b** shows cryo-EM density of the SNX17 CT peptide; **c**, **d** shows surface conservation calculated with ConSurf[63], with color-to-white gradients representing the most (ConSurf score = 9) to the least conserved residues (ConSurf score = 1). Contacting residues are shown as sticks. Dotted yellow lines indicate polar interactions. Residues mutated in this study are indicated by a black box. **e** Sequence alignment of human VPS35L and VPS26C with orthologs from indicated representative species. Residues contacting SNX17 are indicated with yellow boxes and arrowheads. Deleterious somatic mutations found in the COSMIC database and mutations tested for binding to SNX17 are indicated. Coomassie blue-stained SDS PAGE gels showing GST-SNX17 (**f**) or MBP-CCDC22-CCDC93 VBD dimer (**g**) pulling down purified Retriever bearing the indicated point mutations in VPS35L or VPS26C. Representative results from at least two independent experiments are shown. Source data for **f** and **g** are provided as a Source Data file.

Table 1 | Cryo-EM data collection and model statistics

	VPS35L-VPS29-VPS26C-SNX17 (EMD-43873)	VPS35L (partial)-VPS26C-SNX17 (EMD-43870)	VPS35L (partial)-VPS29 (EMD-43871)	Composite map (EMD-43872) (PDB 9AU7)
Data collection and processing				
Magnification	105,000			
Voltage (kV)	300			
Electron exposure ($e^-/Å^2$)	64			
Defocus range (μm)	−0.9 to −2.4			
Pixel size (Å)	0.83			
Symmetry imposed	C1			
Initial particle images (no.)	1,009,886			
Final particle images (no.)	227,973			
Map resolution (Å)	3.4	3.35	3.75	
FSC threshold	0.143			
Refinement				
Initial model used				AlphaFold Multimer model (ma-swt4h)
Model composition				
Nonhydrogen atoms				8601
Protein residues				1079
Ligand				0
R.m.s. deviations				
Bond lengths (Å)				0.005
Bond angles (°)				1.026
Validation				
MolProbity score				1.93
Clashscore				13.06
Poor rotamers (%)				0.21
Ramachandran plot				
Favored (%)				95.65
Allowed (%)				4.35
Disallowed (%)				0.00
Protein residues included in the model				VPS35L:115-131, 180-253, 264-349, 352-738, 742-755, 768-786 VPS29: 3-186 VPS26C: 1-53, 63-146, 150-297 SNX17: 458-470

interaction mechanism is conserved through evolution. Moreover, at least three of these SNX17-interacting residues have been noted to be mutated in cancer (Fig. 3e, indicated by pink dots)[6], with the resulting missense change predicted to be deleterious.

To validate our structural model, we purified a series of Retriever complexes in which we mutated individual residues that make critical contacts with the SNX17 tail, either from the VPS35L or VPS26C side. We then used GST pull-down experiments to examine how these mutations affect the SNX17-Retriever interaction. Consistent with our structure, all mutations abolished the binding to GST-SNX17 (Fig. 3f). Importantly, the disruption of the binding was not due to mis-assembly of Retriever, as the mutant complexes behaved similarly to their wild-type (WT) counterparts during protein expression, purification, and size-exclusion chromatography (Supplementary Fig. 1b, c). Furthermore, the mutations did not affect the binding of Retriever to the CCDC22/CCDC93 VPS35L binding domain (VBD) dimer (Fig. 3g; Supplementary Fig. 1d), which is mediated by different conserved surfaces on the VPS29-bound end of the complex, away from the SNX17 binding pocket (Supplementary Fig. 4a), further supporting that the mutations were specific in disrupting the binding to SNX17. Thus, we postulate that the identified SNX17-binding pocket (hereafter named SBP) is an evolutionarily conserved surface required for binding to SNX17.

Disrupting the SBP alters SNX17 binding in cells

Having defined the SBP as required for in vitro binding between Retriever and SNX17, we examined whether this interaction mechanism held true in cells using co-immunoprecipitation experiments. First, we observed that in transfected HEK293T cells, different mutations in the SBP impacted the binding between SNX17 and Retriever to varied extents. The mutations V205D and R248M in VPS35L substantially weakened the interaction, while other mutations (N279L and W280Y) had minimal effects (Fig. 4a). Combining the V205D and R248M mutations (denoted as DM for double mutant hereafter) had a more profound impact on SNX17-Retriever binding (Fig. 4b). Next, using immunoprecipitation in the reciprocal direction, we further confirmed the significant contribution of VPS35L SBP residues (N279, W280, V205, and R248) to the interaction between Retriever and SNX17 (Fig. 4c), with VPS35L DM displaying the most robust impairment. Importantly, all the mutants tested retained normal interactions in cells with the Retriever subunits VPS29 and VPS26C, as well as normal interactions with the CCC complex (CCDC22 and DENND10) (Fig. 4c), confirming our in vitro results that the mutations specifically disrupted Retriever binding to SNX17 without affecting other regions of Retriever.

Finally, we complemented a previously established *VPS35L* knockout (KO) HeLa cell line[8] and generated polyclonal sublines stably

https://doi.org/10.1038/s41467-024-54583-6

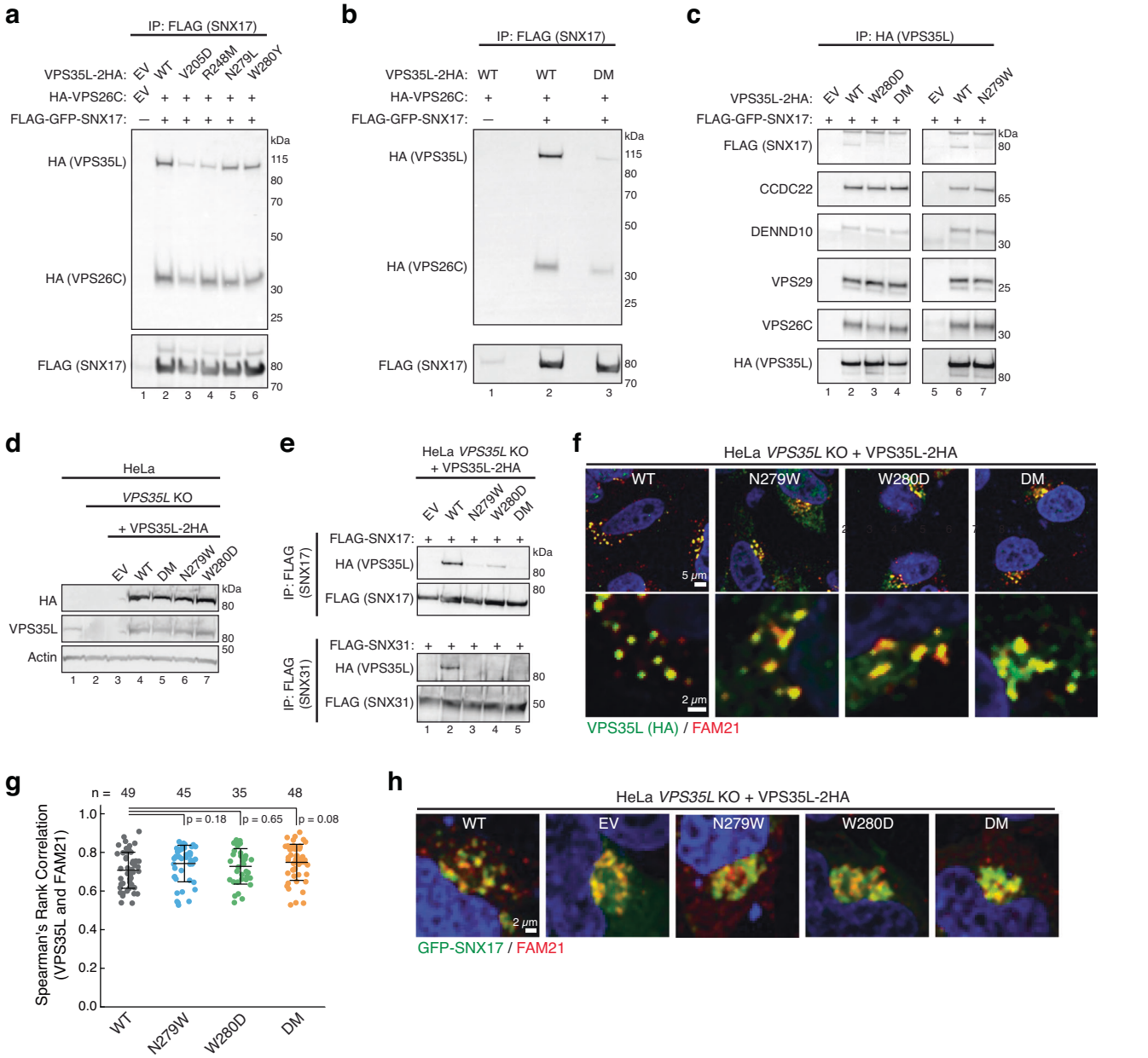

Fig. 4 | Disrupting the SBP impairs SNX17 and SNX31 binding in cells. **a**, **b** Immunoprecipitation of SNX17 (FLAG) followed by immunoblotting for VPS35L and VPS26C (HA) in HEK293T cells transfected with the indicated expression vectors. EV, empty vector; DM, double mutant. **c** Immunoprecipitation of VPS35L (HA) followed by immunoblotting for SNX17 (FLAG) and indicated protein components of the CCC and Retriever complexes in HEK293T cells transfected with indicated SNX17 and VPS35L variants. **d** Immunoblotting analysis for endogenous and stably expressed VPS35L in the indicated HeLa cell lines derived from a *VPS35L* knockout (KO) rescued with the indicated variants of VPS35L or an empty vector (EV) control. The parental HeLa cell line used to derive the VPS35L knockout line is included for comparison. **e** Immunoprecipitation of SNX17 (top) or SNX31 (bottom) after transfection in the indicated HeLa cell lines, followed by immunoblotting for VPS35L (HA). Representative confocal images (**f**) and quantification of colocalization (**g**) derived from concurrent immunofluorescence staining for VPS35L (HA, green) and the endosomal marker FAM21 (red) in HeLa cells shown in **e**. In **g**, each dot represents an individual cell, with number of cells in each group indicated above the graph. Mean and standard deviation are shown. One-way ANOVA with Dunnett's correction was used. NS not significant. **h** Representative confocal images showing concurrent immunofluorescence staining for GFP-SNX17 (green) and the endosomal marker FAM21 (red) in HeLa cells shown in **e** and transfected with GFP-SNX17. All western blot experiments and imaging experiments were performed at least twice. Representative results are shown. Source data for **a**–**e**, **g** are provided as a Source Data file.

re-expressing different HA-tagged VPS35L variants, including WT, N279W, W280D, and DM, or a control line transfected with an empty vector (EV) (Fig. 4d). Using these lines, we examined whether the SBP is required for SNX17 as well as SNX31 binding. SNX31 is a homolog of SNX17 (40% identity between human proteins) expressed only in very few cell types. SNX31 was previously found to bind to Retriever in a manner that also required its CT leucine residue[4]. Our co-immunoprecipitation experiments demonstrated that both SNX17 and SNX31 bound to VPS35L WT but not to the SBP mutants (Fig. 4e), indicating that the SBP is required for Retriever interactions with both proteins.

Retriever-SNX17 binding is not required for their endosomal localization

Next, we examined the potential impact of decoupling Retriever from SNX17 on the localization of these proteins in cells. Using

https://doi.org/10.1038/s41467-024-54583-6

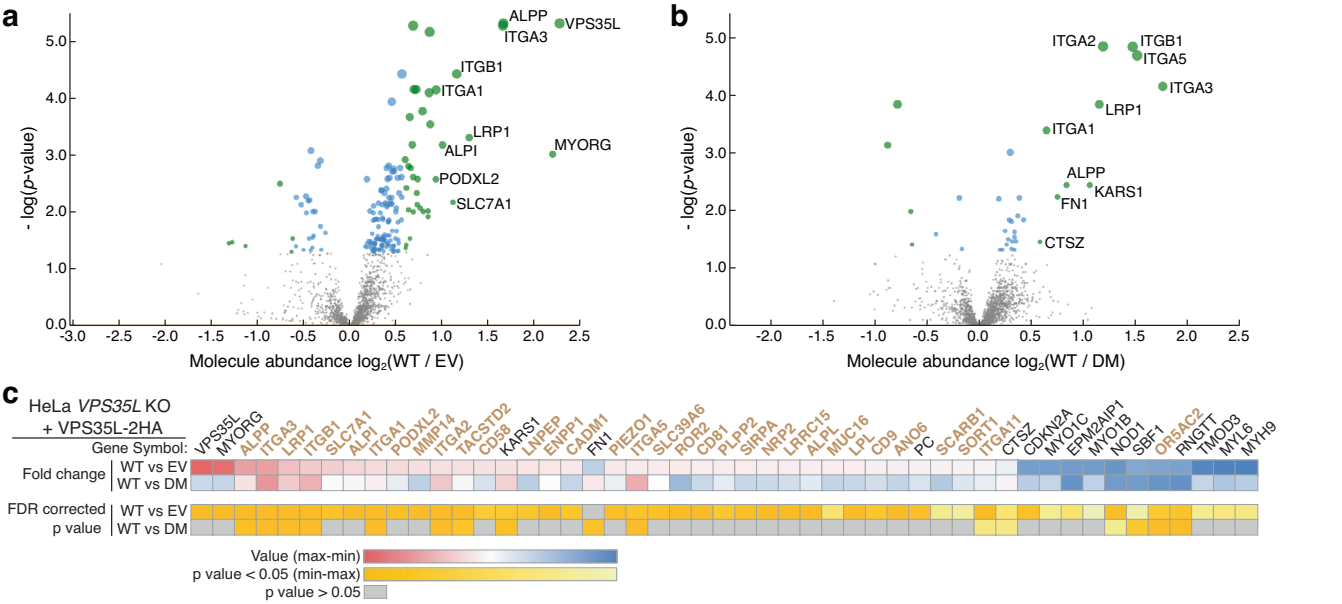

Fig. 5 | Disrupting the SNX17-Retriever interaction impairs PM protein homeostasis. Volcano plots summarizing TMT-based proteomic quantification of plasma membrane proteins, comparing WT to EV cells (**a**), and WT to DM cells (**b**). This experiment was performed once, with each group consisting of six biological replicates. Two-sided Student's *t* test and Benjamini–Hochberg false discovery rate (FDR) correction were applied in data analyses. Colored dots (blue or green) denote proteins with FDR-corrected *p* value < 0.05; green dots depict hits that also had >2-fold change. Dot size is proportional to the position on the *y* axis (depicting statistical significance). **c** Heat map of PM protein abundance quantified by TMT-based proteomics after surface biotinylation and streptavidin purification, using indicated HeLa stable cell lines (shown in Fig. 4d). Only proteins whose abundance was significantly different between WT and EV lines (*p* value < 0.05) are displayed. Membrane proteins are denoted in brown font. Detailed proteomic data are provided in Supplementary Data 1 and deposited in MassIVE repository, as detailed in the data availability section.

immunofluorescence staining in the aforementioned stable lines shown in Fig. 4d, we found that the re-expressed VPS35L was localized to FAM21-positive endosomes regardless of mutations in the SBP (Fig. 4f, g). Reciprocally, SNX17 localization in these cells was assessed after transfection of GFP-SNX17, showing that endosomal localization of SNX17 appeared normal in EV cells and was not impacted by disruption of the SBP (Fig. 4h). Thus, endosomal recruitment of VPS35L and SNX17 are both independent of Retriever-SNX17 complex formation.

Disruption of the SBP alters PM homeostasis

Next, we examined the functional consequence of disrupting the Retriever-SNX17 interaction on endosomal protein sorting and PM protein homeostasis. To assess this, we first utilized surface biotinylation, protein isolation, and mass spectrometry, coupled with tandem mass tag (TMT) quantification, to compare the PM proteomes in HeLa cells re-expressing VPS35L WT or the DM mutant, or the knockout line (complemented with EV). This method detected 40 proteins that were significantly reduced in *VPS35L*-deficient cells (EV) after surface biotinylation (Fig. 5a, c; Supplementary Data 1). These proteins are primarily PM proteins and include six integrins and LRP1, which are known cargoes of SNX17[4,31,35,36]. Remarkably, many cargoes reduced in EV cells were similarly reduced in VPS35L DM mutant cells (Fig. 5a–c), suggesting that the Retriever-SNX17 interaction plays a major role in Retriever-mediated cargo sorting and recycling to the PM.

To validate the PM proteomics result, we used immunofluorescence staining to directly evaluate the cellular localization of Integrin α5 (ITGA5). Consistent with the proteomics data, ITGA5 exhibited reduced staining at the PM and accumulation in FAM21-positive endosomes of EV cells (Fig. 6a). Importantly, SBP mutations in VPS35L led to a comparable phenotype, with EV and SBP mutants showing significant endosomal trapping of ITGA5 (Fig. 6b). The same analysis of another SNX17 cargo, Integrin β1 (ITGB1), revealed a similar pattern of endosomal trapping in cells lacking VPS35L (EV) or expressing VPS35L with SBP mutations (Fig. 6c, d). Direct assessment of PM levels of ITGB1 by flow cytometry analysis confirmed that VPS35L EV and DM cells exhibit reduced surface levels of this integrin (Fig. 6e–g). Associated with the endosomal trapping phenotypes was an altered morphology of FAM21-positive endosomes, displaying enlarged endosomal domains and coalescence in the perinuclear region (Fig. 6h). The coalescence phenotype, quantified as area of FAM21-positive endosomes per cell, showed significant alterations in VPS35L deficiency (EV) as well as in all SBP mutants tested (Fig. 6i). Thus, decoupling Retriever from SNX17 had a profound effect on the endosomal recycling of various PM proteins and the associated morphological alterations within endosomal compartments.

SBP mutations reveal other acidic tail partners of Retriever

Next, we assessed the range of protein-protein interactions for VPS35L WT and compared its interacting partners with the DM variant. To accomplish this, we immunoprecipitated VPS35L from the corresponding HeLa cell lines and identified interacting partners using mass spectrometry in an unbiased manner. Using a 10-fold enrichment over the EV knockout as a threshold, coupled with statistical analysis corrected for multiple testing, we identified 14 potential VPS35L interacting proteins (Fig. 7a; Supplementary Data 2). This analysis readily identified known components of the Retriever and CCC complexes (Fig. 7a), although we could not detect SNX17, possibly due to its low cellular abundance, low stoichiometry or affinity of binding, or poor peptide ionization. Our method also identified several proteins not previously reported to be partners of Retriever, such as LRMDA and ADGRE3 (Fig. 7a).

Intriguingly, we found that LRMDA (leucine rich melanocyte differentiation associated) preferentially bound to VPS35L WT but not the DM mutant (Fig. 7b). LRMDA contains an NT leucine-rich repeat (LRR) domain and a CT unstructured tail (Fig. 7c). Immunoprecipitation and Western blot confirmed that LRMDA only interacted with VPS35L WT but not the SBP mutants (Fig. 7d). Immunoprecipitation in Lenti-X

https://doi.org/10.1038/s41467-024-54583-6

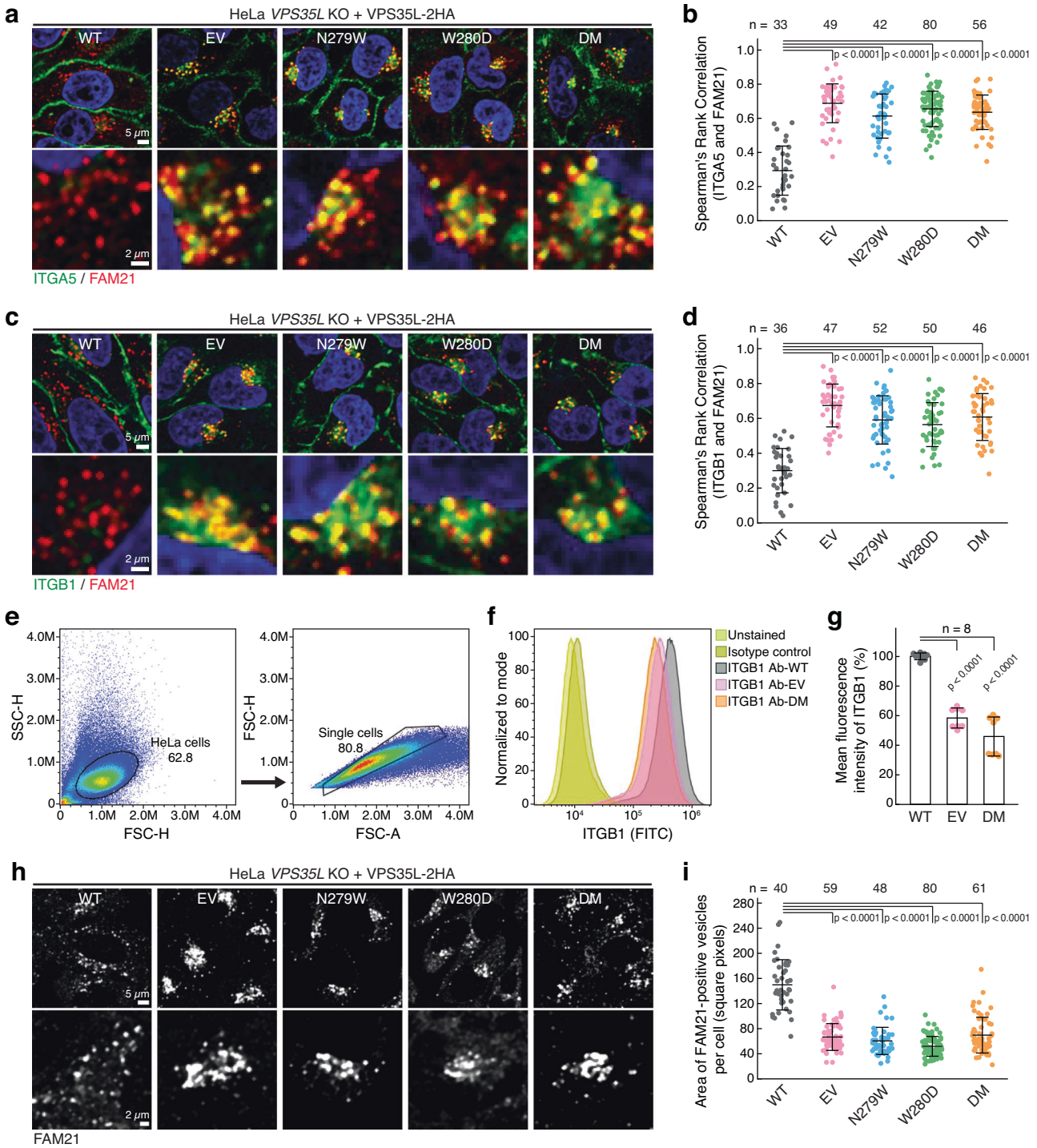

Fig. 6 | Disrupting the SNX17-Retriever interaction impairs PM protein trafficking and endosomal morphology. Representative confocal images (**a**) and quantification of colocalization (**b**) derived from concurrent immunofluorescence staining for the cargo protein ITGA5 (green) and the endosomal marker FAM21 (red) in the indicated cell lines. **c**, **d** Similar to **a**, **b** but focusing on the cargo protein ITGB1 (green). Flow cytometry analysis of surface ITGB1 in indicated HeLa cell lines, showing scatter plots depicting gating (**e**), a representative histogram depicting ITGB1 surface staining (**f**), and mean fluorescence intensity compared to WT cells in the indicated HeLa cell lines (**g**). In **g**, aggregate data from 2 independent experiments are shown, with each dot representing a biological replicate. Representative confocal images (**h**) and quantification of the area of FAM21-positive endosomes (**i**) derived from immunofluorescence staining of FAM21 in the indicated HeLa stable cell lines. In all quantifications, each dot represents an individual cell, with number of cells in each group indicated above the graph. Mean and standard deviation are shown. One-way ANOVA with Dunnett's correction was used. All imaging and FACS experiments were performed at least twice. Representative results are shown.

293T cells transfected with the full length (FL), NT LRR, and CT tail of LRMDA revealed that the CT tail is both necessary and sufficient for binding to Retriever (Fig. 7e), analogous to SNX17.

Comparing the CT tail sequences of validated SBP-dependent binders (SNX17, SNX31, and LRMDA) across various representative species revealed significant homology among their extreme C-terminus (Fig. 8a), suggesting a potentially shared mechanism of binding. This homology can be summarized as an evolutionarily conserved consensus motif comprising the last six residues, which we initially denoted as [ILF]-x-a-a-a-L, with "x" for any amino acid and "a"

https://doi.org/10.1038/s41467-024-54583-6

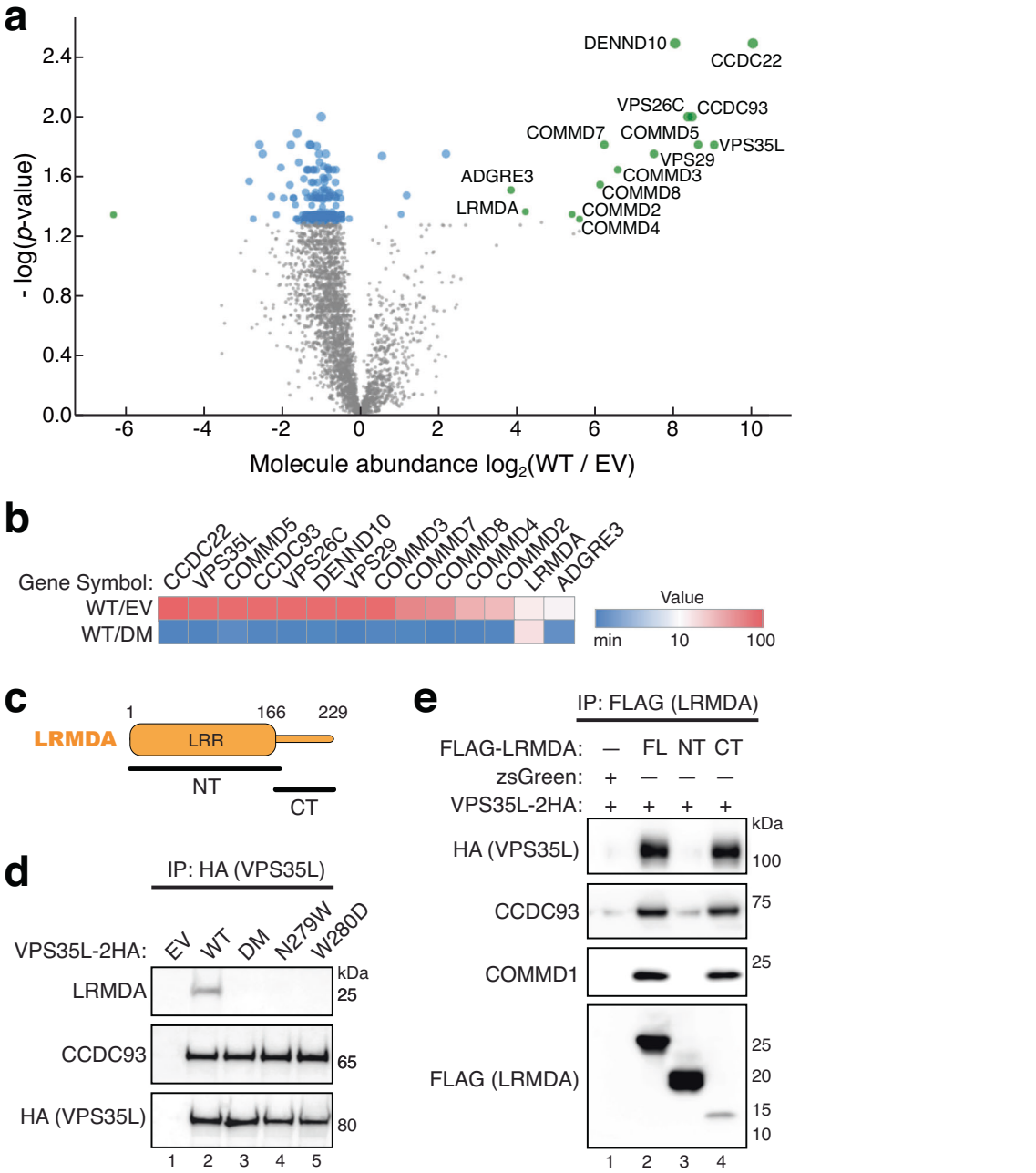

Fig. 7 | Interactome analysis reveals that LRMDA similarly binds to Retriever. Volcano plot (**a**) and heat map (**b**) of VPS35L-interacting proteins quantified by mass spectrometry after coimmunoprecipitation of HA-tagged VPS35L, using indicated HeLa stable cell lines shown in Fig. 4d. Two-sided Student's *t* test and Benjamini–Hochberg false discovery rate (FDR) correction were applied in data analyses. Colored dots (blue or green) denote proteins with FDR-corrected *p* value < 0.05; green dots depict hits that also had >10-fold change between WT and EV control samples. Dot size is proportional to the position on the *y* axis (depicting statistical significance). Protein spectral counts, fold change between indicated cells, and corresponding p-values are depicted. **c** Cartoon presentation of LRMDA domain organization and constructs used in **e**. **d** Immunoprecipitation of VPS35L (HA) followed by immunoblotting for LRMDA and CCDC93 in indicated stable HeLa cell lines. **e** Immunoprecipitation of LRMDA full-length (FL), NT, and CT in Lenti-X 293 T cells, followed by immunoblotting for indicated Retriever and CCC subunits. The experiment in **a** and **b** was performed once, with three biological replicates included in each group. Detailed proteomic data are provided in Supplementary Data 2 and deposited in MassIVE repository as detailed in the data availability section. Western blot experiments in **d** and **e** were performed three times. Representative results are shown.

for acidic residues (Fig. 8a, black box). The sequences preceding this motif lack a discernable pattern, suggesting the decisive role of this six-residue motif in binding to Retriever. Note that this six-residue motif is located just distal to the conserved NxxY/F motif in SNX17, which is absent in SNX31 and LRMDA (Fig. 8a, pink).

In the CT six-residue motif, the last L seemed the most invariant, followed by the first I residue, which could also be L or F in several species. The three central acidic residues could be a combination of D, E, N, and Q, while the "x" position could be various amino acids. To define this motif's composition more precisely, we performed extensive mutagenesis across the CT tail and tested how mutations affected the binding to Retriever (Fig. 8b). We found that mutations of the terminal L abrogated the binding, consistent with the sequence analysis in Fig. 8a. However, the −2 and −3 positions tolerated various

https://doi.org/10.1038/s41467-024-54583-6

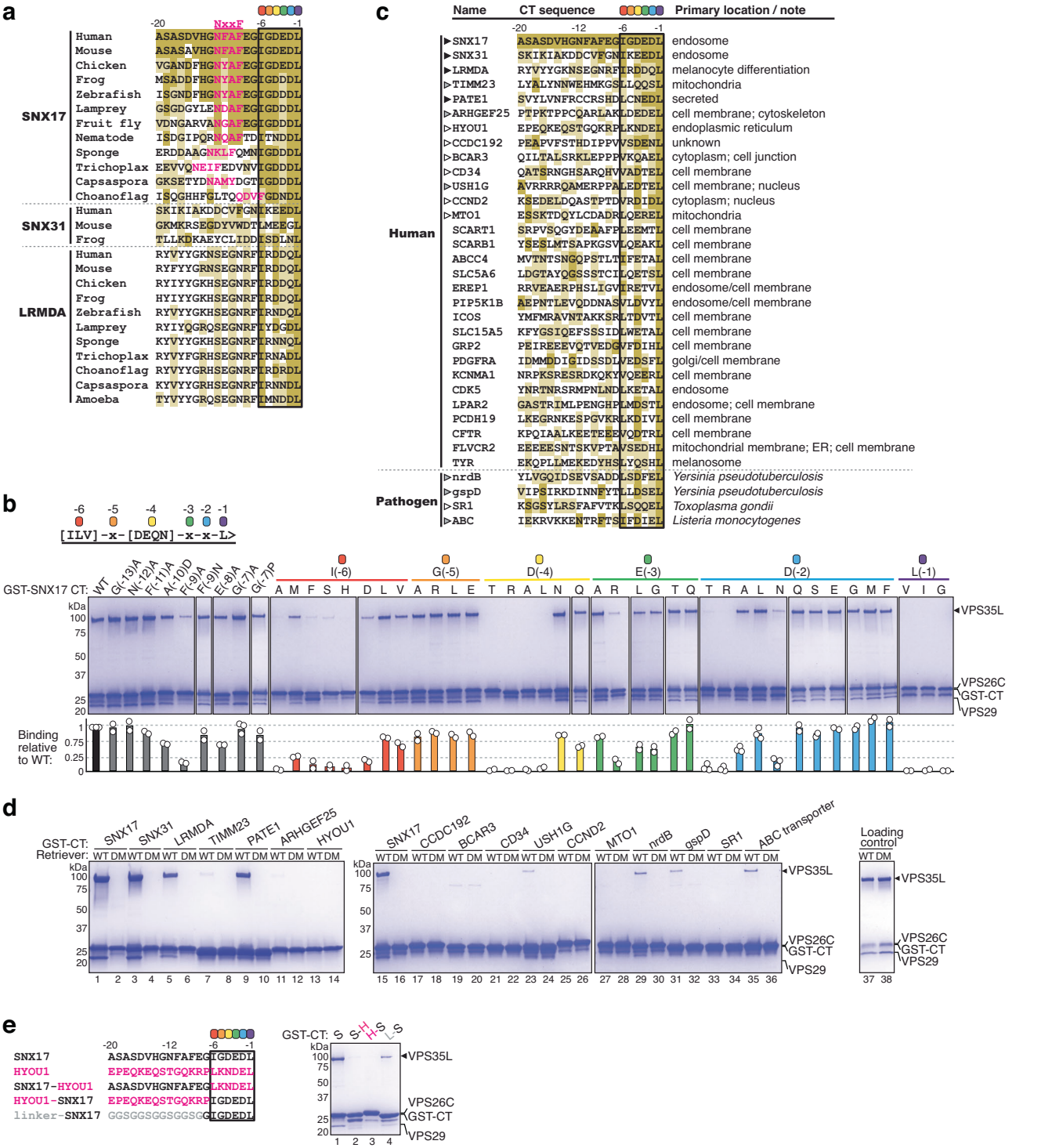

Fig. 8 | Sequence analysis reveals a consensus C-terminal Retriever-binding motif. a Sequence alignment of the CT tail of indicated proteins across representative species. Gold, light gold, and white shading denote sequences identical to, similar to, and not conserved with the human SNX17 CT sequence, respectively. The identified 6-residue acidic sequences are highlighted by the black box, with each position denoted by a colored dot corresponding to the residues mutated in **b**. The conserved NxxF motifs are marked in pink, with the assignment of QDVF in the Choanoflagellate sequence based on AlphaFold predictions. **b** Definition of the consensus RICT motif and Coomassie blue-stained SDS PAGE gels showing in vitro pull-down of Retriever by GST-SNX17 CT tails containing indicated point mutations. Binding signals of VPS35L bands are quantified and normalized to the WT CT and shown beneath corresponding mutations. Each dot represents a repeat ($n = 2$ or 3). **c** Sequence alignment of the CT tail of indicated proteins in humans or pathogens containing a RICT motif at the C-termini of unstructured tails. Gold, light gold, and white shading denote sequences identical to, similar to, and not conserved with the human SNX17 CT sequence, respectively. Black and gray arrowheads indicate strong and weak binding in the pull-down assay shown in **d**, respectively. White arrowheads indicate no detectable interaction. Proteins without an arrowhead were not tested. **d** Coomassie blue-stained SDS PAGE gels showing in vitro pull-down of Retriever WT vs. the DM mutant by GST-tagged CT of the indicated proteins. **e** Sequences and Coomassie blue-stained SDS PAGE gel showing in vitro pull-down of Retriever by indicated chimera CT tails. Representative results from two independent experiments are shown for RICT motif screening and chimera CT tail pull-down.

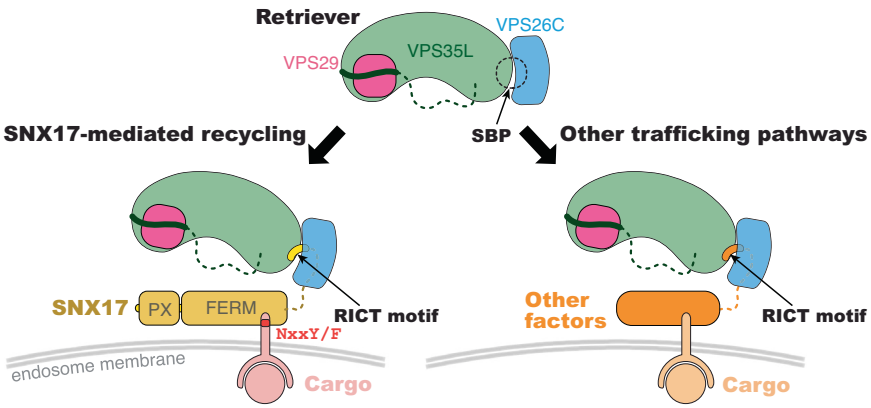

Fig. 9 | Schematic of Retriever-mediated endosomal recycling. Our study suggests that Retriever could use the same SNX17-binding pocket (SBP) to interact with additional factors that contain the Retriever interacting C-terminal tail (RICT) motif. The interaction with SNX17 tethers Retriever to many cargoes recognized by SNX17 through NxxY/F motifs in their cytoplasmic tails (left), while the interaction with other factors can potentially link Retriever to distinct cargoes, recycling pathways, or cellular destinations (right).

other amino acids, with D(−2) tolerating most mutations except for T, R, and N, and E(−3) tolerating most mutations except for R. In contrast, the −4 position could only accommodate D, N, Q (and likely E). The −5 position tolerated all tested mutations, while the −6 position could only tolerate small hydrophobic residues, including I, L, and V, consistent with the sequence analysis. Outside of the last six residues, NT mutations at most positions did not impact binding, except at the −9 position and, to a less extent, the −10 position (Fig. 8b), suggesting that the sequences preceding the CT motif also play a role in binding, in agreement with the observation of 12 residues of SNX17 CT in the SBP. Combining these results, we redefined the consensus motif as [ILV]-x-[DEQN]-x-x-L and named it Retriever Interacting C-terminal Tail (RICT).

Based on the RICT motif, we searched transmembrane or membrane-associated proteins from humans and several pathogens and identified additional proteins containing a sequence in an unstructured C-terminal tail that conforms with the consensus for RICT (Fig. 8c). These proteins have diverse membrane localizations and were previously not shown to bind to Retriever. To validate our prediction, we selected several proteins and purified their last 20 amino acid sequences fused to GST. Similar to SNX17, the CT tails of SNX31, LRMDA, and PATE1 showed robust binding to Retriever in vitro, while TIMM23, ARHGEF25, USH1G, and pathogenic proteins nrdB (*Y. pseudotuberculosis*), gspD (*Y. pseudotuberculosis*), and amino acid ABC transporter permease (*L. monocytogenes*) showed weaker interactions (Fig. 8c, d). Notably, all interactions were abrogated by the DM mutation, confirming that they use the same mechanism to interact with the SBP of Retriever (Fig. 8d).

To understand why some CT tails containing a well-defined RICT motif did not show binding, we speculated that the overall interaction is influenced not only by the RICT motif but also by the entire sequence context. To test this hypothesis, we designed chimeric CT tails by swapping the NT sequence and the CT RICT motif from a binding protein, SNX17, with corresponding sequences from a non-binder, HYOU1, or with a featureless flexible (GGS) linker sequence (Fig. 8e, left panel). We found that replacing either the NT sequence or the CT RICT motif of the SNX17 CT tail with corresponding HYOU1 sequences abolished Retriever binding (Fig. 8e, lanes 2, 3). This demonstrates that the RICT motif of HYOU1 cannot bind to Retriever and that the NT sequence preceding the RICT motif in the HYOU1 CT tail prevents SNX17's RICT motif from binding to Retriever. Interestingly, replacing the NT sequence of the SNX17 tail with a (GGS) linker only weakened its binding to Retriever but did not abolish it, indicating that the native NT sequence of SNX17 tail promotes the binding, while the NT sequence of HYOU1 disrupts the binding (Fig. 8e, lane 4). Together, we conclude that although the six-residue RICT motif is both necessary and sufficient for binding to Retriever, the overall interaction is determined by two factors: 1) the exact amino acid combination within the RICT motif, and 2) the sequence preceding the RICT motif. This emphasizes the importance of experimentally validating the predicted RICT-containing proteins in future studies.

Discussion

Our study provides a pivotal advance in our understanding of Retriever-mediated endosomal cargo recycling. Unlike the well-studied Retromer[25,26,34], the precise mechanisms of cargo selection by Retriever have remained elusive[37]. Our findings elucidate how the cargo-recognition factor SNX17 uses its C-terminal tail to anchor into a conserved surface formed by the VPS35L and VPS26C subunits of Retriever (Fig. 9, left). This is in line with a recent study derived from AlphaFold structural prediction and mutagenesis validation[38]. Furthermore, we have identified other regulatory factors that interact with Retriever through the SBP and via similar CT tails, suggesting that the SBP is a critical surface that connects Retriever to other cellular functions beyond SNX17-dependent cargo recycling[8] (Fig. 9, right).

We emphasize that despite sharing remote homology with Retromer and SNX27, Retriever and SNX17 operate through very distinct mechanisms. Notably, the residues surrounding the binding pocket on both the VPS35L and VPS26C sides are highly conserved across species, representing one of the most conserved surfaces on Retriever (Supplementary Fig. 4a). This remarkable conservation underscores the evolutionary and functional significance of the interaction between Retriever and SNX17, as well as other RICT-containing factors.

Another striking observation is that disrupting the Retriever-SNX17 interaction has profound consequences on PM protein homeostasis, affecting cellular signaling and potentially having clinical implications. This is evidenced by our proteomic and cellular analyses, as well as the association between somatic mutations at the SNX17 binding pocket and human cancers. Mutations at these residues disrupt the Retriever-SNX17 interaction in our experimental system, suggesting that the cancer-associated mutations may act by perturbing the homeostasis of crucial cargoes involved in cell adhesion, proliferation, or metabolism. This binding pocket, therefore, offers a promising target for the development of therapeutic interventions or small molecule drugs to modulate cellular signaling dynamics.

Our proteomic and cellular studies indicate that SNX17 does not constitutively bind to Retriever. It is plausible that the binding could be modulated by various parameters, such as SNX17's expression level, post-translational modifications, cargo binding, cargo membrane

density, and cellular localization. In particular, our data indicate that SNX17's ability to bind to Retriever is autoinhibited through intramolecular interactions, and this autoinhibition is relieved by cargo binding, indicating that cargo recognition and Retriever recruitment to cargoes are synergistic processes. This notion is also supported by a recent study similarly showing autoinhibition of SNX17[38]. Interestingly, various sorting nexin proteins, such as SNX27[29], SNX3[26,39], SNX1-SNX6[28], and SNX1-SNX5[40], operate similarly, being autoinhibited in the basal state, with cargo binding enhancing their association with Retromer or membranes. Although SNX31 and LRMDA, two other confirmed SBP-binding proteins, lack the NxxY/F motif and are not predicted by AlphaFold to be autoinhibited, they may use distinct mechanisms to regulate the accessibility of their CT tails. It's worth noting that although our in vitro results suggest that the PX domain binding to PI(3)P does not directly impact the autoinhibitory state, it remains possible that membrane recruitment through PI(3)P binding can indirectly promote Retriever-cargo interaction by facilitating SNX17 recruitment to microdomains enriched with both Retriever and cargo proteins. Our structure also suggests that the SNX17-Retriever interaction can be regulated by post-translational modifications. For example, based on PhosphoSitePlus[41], two key residues at the SBP could be potentially modified, including acetylation of K14 in VPS26C and ubiquitylation of K204 in VPS35L, which could disrupt SNX17 binding. In addition, several residues in SNX17 CT near the NxxY/F motif could be phosphorylated, including S434, S437[42], and S440, which may modulate the autoinhibition mechanism. Finally, a recent study showed that SNX17 CT could interact with the PDZ domain of a group of PDLIM proteins, which could provide a regulatory mechanism to decouple SNX17 and its cargoes from Retriever[43].

The identification of other factors containing the SNX17 homologous acidic tail sequences (i.e., the RICT motif) suggests a versatile role for the binding pocket. These additional factors may act as competitors of SNX17 and connect Retriever to a broader range of recycling pathways, cargoes, or other cellular locations and functions. These include not only proteins in the host cells, but also effectors from pathogens, which might exploit the host trafficking system by hijacking the Retriever-SNX17 interaction and compromising host cellular functions to create a niche or augment pathogen fitness. In summary, our research not only elucidates a key mechanism in endosomal trafficking but also opens the door for further exploration into the biological significance of other Retriever-ligand interactions.

Methods

Plasmids

All constructs were created using standard molecular biology procedures and verified by Sanger sequencing. Detailed information about constructs for recombinant protein production and mammalian expression, recombinant protein sequences, and DNA oligonucleotides for construct generation can be found in Supplementary Tables 1, 2, and 3, respectively. The ORFs of human VPS35L and VPS26C were previously described[6,21,44]. The mammalian expression vector for SNX17 was previously described[45]. SNX31 mammalian expression vector was designed by GeneArt at Thermo Fisher Scientific. For insect cell expression of Retriever, human full-length VPS35L (untagged, synthesized as a codon-optimized GeneString from Thermo Fisher to improve expression), VPS26C (untagged), and VPS29 (isoform 2) containing a C-terminal $(GGS)_2$-His_6 tag were cloned in a modified pFastBac™ vector for insect cell expression as previously described[6]. For bacterial expression of isolated VPS26C, codon-optimized GeneString (Thermo Fisher) was cloned in a pMalC2Tev vector[6]. Bacterial expression vector of GST-SNX17 was previously described[31]. Bacterial expression vectors of CCDC22 VBD and CCDC93 VBD were previously described[6]. The CT 20 amino acids of SNX17, SNX31, LRMDA, TIMM23, PATE1, ARHGEF25, HYOU1, CCDC192, BCAR3, CD34, USH1G, CCND2, MTO1, nrdB2, gspD, SR1, and amino acid ABC transporter were codon-optimized and cloned into a pGexTev vector using PCR.

E. coli strains for protein expression

Standard, commercial *E. coli* strains used in this study include Mach1^{T1R} (Thermo Fisher) and BL21 (DE3)^{T1R} (Sigma), and are grown in Luria-Bertani medium using standard molecular biology conditions.

Insect cell lines for protein expression

Sf9 cells (Expression System) were maintained in Sf-900™ II serum-free medium (Thermo Fisher) and used for baculovirus preparation and large-scale expression.

Cell culture

HEK293T (Cat # CRL-3216) and HeLa (Cat # CCL-2) cell lines were obtained from the American Type Culture Collection (Manassas, VA). Lenti-X 293T cells (Cat #632180) were obtained from Takara. All cell lines were cultured in high-glucose Dulbecco's modified Eagle's medium (DMEM) containing 10% fetal bovine serum (FBS) and 1% penicillin/streptomycin at 37 °C with 5% CO_2. Periodic PCR-based testing for Mycoplasma spp. was conducted to ensure culture purity. A HeLa line with VPS35L deficiency was previously described[8] and these cells were complemented using a lentiviral vector to express HA tagged VPS35L protein versions as indicated.

Transfection and lentiviral methods

HEK293T or Lenti-X 293T cells were transfected using Lipofectamine 2000 (Life Technologies) or PolyJet (SignaGen), respectively, and cultured for either 24 or 48 h before analysis. VPS35L HeLa knockout cells were reconstituted with HA empty vector or various HA-tagged VPS35L using a lentivirus system. Lentivirus experiments followed a standard protocol as previously described for viral vector production and selection[46,47].

Immunofluorescence staining

We followed protocols previously described[8,21]. Briefly, cells were fixed with cold fixative (4% paraformaldehyde in PBS) for 18 min at room temperature in the dark, followed by 3-min permeabilization using 0.15% Surfact-Amps X-100 (28314, Thermo Fisher) in PBS. Samples were then incubated overnight at 4 °C in a humidified chamber with primary antibodies in immunofluorescence (IF) buffer (Tris-buffered saline plus human serum cocktail). After three washes in PBS, samples were incubated with secondary antibodies (1:500 dilution in IF buffer) for 1 h at room temperature or overnight at 4 °C in a humidified chamber. After four washes in PBS, coverslips were mounted on slides with SlowFade Anti-fade reagent (Life Technologies). Primary and secondary antibodies used are provided in Supplementary Table 4. Images were obtained using an A1R confocal microscope (Nikon, ×60/1.4 oil immersion objective) operated by the NIS-Elements A1R (Nikon) software v5.42.03. Fluorescence signal values were quantified using Fiji v1.54 f (ImageJ, NIH). Data were processed with Excel (Microsoft) and plotted with Prism v9.5.1 (GraphPad) or a Python web application https://biochempy.bb.iastate.edu. Each dot in the graphs represents the value from a single cell, with the horizontal bar indicating the mean and the error bars representing the standard error of the mean (SEM). Spearman's Rank correlation coefficient was measured using EzColocalization Fiji Plugin within manually outlined regions of interest (ROIs).

Mammalian protein extraction, immunoblotting, and immunoprecipitation

For most experiments, whole cell lysates were prepared using Triton X-100 lysis buffer (25 mM HEPES, 100 mM NaCl, 10 mM DTT, 1 mM EDTA, 10% Glycerol, 1% Triton X-100) supplemented with

protease inhibitors (Roche). Immunoprecipitation, SDS-PAGE, and immunoblotting experiments were performed largely as previously described[8]. Specifically, for LRMDA immunoprecipitation, 48 h after transfection, cells were harvested in NP-40 lysis buffer and mixed with anti-FLAG M2 magnetic beads (Sigma-Aldrich, Cat# F4799) for 2 hours at 4 °C. The beads were washed 4 times in NP-40 lysis buffer, and the bound proteins were eluted with 150 µg/mL 3×Flag (Sigma-Aldrich, Cat# F4799) at 4 °C for 1.5 h. Western blot images were collected using ChemiDoc and Image Lab v6.1.0 (Bio-Rad). Antibodies used are detailed in Supplementary Table 4.

Cell surface biotinylation

Cell surface biotinylation was performed as previously reported[21]. Briefly, cells were incubated at 4 °C with Sulfo-NHS-SS-biotin (Pierce) in biotinylation buffer (10 mM triethanolamine, 150 mM NaCl, 2 mM $CaCl_2$, pH 8.0). After 30 min, cells were lysed in Tris-lysis buffer (50 mM Tris-HCl, pH 7.4, 150 mM NaCl, 1% NP-40, 0.5% Na deoxycholate, 5 mM EDTA, 5 mM EGTA) supplemented with Halt Protease/Phosphatase inhibitor (Thermo Fisher). Biotinylated proteins were captured using nanolink Streptavidin magnetic beads (Solulink) and washed three times with the same lysis buffer, once with high salt buffer (50 mM Tris-HCl, pH 7.4, 500 mM NaCl), and once with low salt buffer (10 mM Tris-HCl, pH 7.4, 5 µM Biotin). Proteins on the beads were eluted using at the elution buffer (PBS, 6 M urea, 0.2% SDS (v/w) containing 100 mM DTT at 65 °C for 30 min. For TMT proteomics, the eluted proteins were directly submitted in solution to the UT Southwestern Proteomics core facility.

Protein affinity purification

Knockout cells expressing HA-tagged VPS35L were grown on culture dishes and lysed in Triton-X lysis buffer. Clarified cell lysates containing equal amounts of protein were added to HA-resin to capture HA-tagged proteins. HA beads were washed using lysis buffer and eluted using 3 x LDS/DTT gel loading buffer at 95 °C. Eluted proteins were analyzed by SDS-PAGE and LC-MS/MS mass spectrometry at the UT Southwestern Proteomics core.

Proteomic interactome and cell surface analysis

Potential interacting proteins were identified by comparing protein abundance ratios to reveal which proteins were enriched relative to the empty vector (EV) samples, with an arbitrary cutoff of at least 10-fold enrichment. The experiment was performed once, with 3 biological replicates per group. Plasma membrane protein quantification was performed through TMT-based quantification (see below), comparing protein abundance between WT cells and either EV cells or DM expressing cells, focusing on at least 2-fold differences between groups. The experiment was performed once, with 6 biological replicates per group. After reduction with DTT and alkylation with iodoacetamide (Sigma–Aldrich), samples were digested overnight with trypsin (Pierce). After solid-phase extraction cleanup with an Oasis HLB plate (Waters), digested samples were injected into an Orbitrap Fusion Lumos mass spectrometer coupled to an Ultimate 3000 RSLC-Nano liquid chromatography system with a 75 µm i.d., 75-cm long EasySpray column (Thermo). Peptides were eluted with a gradient from 1 to 28% buffer B over 90 min. Buffer A contained 2% (v/v) ACN and 0.1% formic acid in water, and buffer B contained 80% (v/v) ACN, 10% (v/v) trifluoroethanol, and 0.1% formic acid in water. The mass spectrometer operated in positive ion mode with a source voltage of 1.8–2.4 kV and an ion transfer tube temperature of 275 °C. MS scans were acquired at 120,000 resolution in the Orbitrap. Up to 10 MS/MS spectra were obtained in the ion trap for each full spectrum acquired using higher-energy collisional dissociation (HCD) for ions with charges 2–7. Dynamic exclusion was set for 25 s after an ion was selected for fragmentation.

For the plasma membrane and interaction proteomics samples, raw MS data were analyzed using Proteome Discoverer v3.0 (Thermo), with peptide identification performed using Sequest HT searching against the reviewed human protein database from UniProt. We set fragment and precursor tolerances at 10 ppm and 0.6 Da, respectively, and allowed three missed tryptic cleavages. Cysteine carbamidomethylation was set as a fixed peptide modification and methionine oxidation as a variable modification. We applied a false-discovery rate (FDR) cutoff of 1% for all peptides.

To analyze protein complex composition in native gel samples, raw MS data were analyzed using MaxQuant v.2.0.3.0, with peptide identification performed against the human protein database from UniProt. We set fragment and precursor tolerances at 20 ppm and 0.5 Da, respectively, and allowed three missed cleavages. We set cysteine carbamidomethylation as a fixed peptide modification, and methionine oxidation and N-terminal acetylation as a variable modification. We used iBAQ quantitation for protein quantitation within each sample.

TMT proteomics

For TMT-based analysis, samples were thoroughly mixed with 25 µL of 10% SDS and 100 mM triethylammonium bicarbonate (TEAB) by vortexing, followed by reduction with 2 µL of 0.5 M tris(2-carboxyethyl) phosphine (TCEP) and incubation at 56 °C for 30 min. Free cysteine thiol groups were then alkylated by adding 2 µL of 500 mM iodoacetamide and incubating in the dark at room temperature for 30 min. Afterwards, 5.4 µL of 12% phosphoric acid and 300 µL of S-Trap (Protifi) binding buffer were added before being loaded onto an S-Trap column. Samples were digested by 1 µg of trypsin and incubation overnight at 37 °C. Digested peptides were eluted, dried and reconstituted in 26 µL of 50 mM TEAB buffer. Equal amounts of peptides from each sample were labeled with TMTpro 18plex reagents (Thermo) based on absorbance at 205 nm using a NanoDrop (Thermo). The six WT samples were labeled with TMTpro reagents 126–129, the six EV samples were labeled with TMTpro reagents 130–132, and the six DM samples were labeled with TMTpro reagents 133–136. After labeling, the reaction was quenched with 5% hydroxylamine, and samples were combined and dried in a SpeedVac. Samples were then cleaned using an Oasis HLB microelution plate (Waters), dried, and reconstituted in 50 µL of 2% acetonitrile, 0.1% TFA.

Peptide samples (1.5 ug) were injected onto an Orbitrap Eclipse mass spectrometer coupled to an Ultimate 3000 RSLC-Nano liquid chromatography system with a 75 µm i.d., 75-cm long EasySpray column (Thermo). Peptides were eluted with a gradient from 1-28% buffer B over 180 min, followed by 28–45% buffer B over 25 min. Buffer A contained 2% (v/v) ACN and 0.1% formic acid in water, and buffer B contained 80% (v/v) ACN, 10% (v/v) trifluoroethanol, and 0.1% formic acid in water. The mass spectrometer operated in positive ion mode with a source voltage of 2.5 kV and an ion transfer tube temperature of 300 °C. MS scans were acquired at 120,000 resolution in the Orbitrap over a mass range of m/z = 400–1600, and top speed mode was used for SPS-MS3 analysis with a cycle time of 2.5 s. MS2 was performed using collisionally-induced dissociation (CID) with a collision energy of 35% for ions with charges 2–6. Dynamic exclusion was set for 25 s after an ion was selected for fragmentation. Real-time search was performed using the reviewed human protein database from UniProt. We set cysteine carbamidomethylation and TMT pro 18plex modification of lysine and peptide N-termini as fixed modifications, and methionine oxidation as a variable modification. We allowed two missed cleavages and up to 3 modifications per peptide. The top 10 fragments for MS/MS spectra corresponding to peptides identified by real-time search were selected for MS3 fragmentation using high-energy collisional dissociation (HCD), with a collision energy of 65%. Raw MS data files were analyzed using both the Sequest HT and Comet nodes within

Proteome Discoverer v3.0 (Thermo), searching against the reviewed human protein database from UniProt. Fragment and precursor tolerances of 10 ppm and 0.6 Da were specified, and two missed cleavages were allowed. The same modifications were used in the search as for the real-time search. The false-discovery rate (FDR) cutoff was 1% for all peptides. Impurity corrections were used for the TMTpro reagents based on the documentation included with the TMTpro reagent kit. *P*-values for protein fold-change across different sample types were adjusted for multiple comparisons using a Benjamini–Hochberg correction.

Flow cytometry

Cells were detached from plates using a cell scraper in 1× PBS and centrifuged at 300 g for 5 min. The cells were resuspended in fresh PBS and rinsed once with a repeat centrifugation step. For ITGB1 staining, cells were immediately processed and resuspended in FACS buffer (PBS, 1% BSA) containing an anti-ITGB1 (CD29) antibody conjugated to FITC for 30 min on ice protected from light. After this, cells were rinsed three times by centrifugation and resuspension in FACS buffer. Samples were processed by the Flow Cytometry core at UT Southwestern using a Cytek Aurora instrument. Data analysis was performed using FlowJo software.

Recombinant protein purification

The Retriever complex or the VPS35L-VPS29 subcomplex was expressed from *Sf9* cells using the Bac-to-Bac system and purified through Ni-NTA affinity, cation exchange, and anion exchange, and size exclusion chromatography essentially as previously described[6]. To improve expression, VPS35L ORF was changed to a codon-optimized sequence from Thermo Fisher. Typical yield was ~1 mg of purified Retriever from 3 liters of *Sf9* culture. SNX17, isolated VPS26C, and SNX17-homologous CT tails were expressed and purified following procedures essentially as previously described[6]. Briefly, proteins were expressed in BL21 $(DE3)^{T1R}$ cells (Sigma) at 18 °C overnight after induction with 1 mM IPTG. GST-tagged SNX17 proteins were purified using Glutathione Sepharose beads (Cytiva) and eluted using 100 mM Tris pH 8.5, 50 mM NaCl, and 30 mM reduced glutathione. The resulting GST-SNX17 proteins were further purified by anion exchange chromatography using a 2-mL Source 15Q column (10 mM Tris pH 8.0 and 5 mM BME in a gradient of 0–400 mM NaCl developed over 40 mL) and size exclusion chromatography using a 24-mL Superdex Increase 200 column [10 mM HEPES pH 7.0, 100 mM NaCl, 5% (w/v) glycerol, and 1 mM DTT]. Untagged SNX17 full-length, PX-FERM, and FERM were expressed with an N-terminal GST tag, purified using Glutathione Sepharose beads as described above. The GST tags were removed using TEV cleavage overnight, further purified by a 2-mL Source 15S column (10 mM MES pH 6.0 and 5 mM BME in a gradient of 0–400 mM NaCl developed over 60 mL), and dialyzed into 10 mM HEPES pH 7.0, 50 mM NaCl, 5% (w/v) glycerol, and 1 mM DTT for pull-down assays. SNX17 point mutants were purified using Glutathione Sepharose beads as described above and then dialyzed into 10 mM HEPES pH 7.0, 100 mM NaCl, 5% (w/v) glycerol, and 1 mM DTT for pull-down assays. SNX17-homologous C-terminal tails were purified using Glutathione Sepharose beads as described above, further purified by a 2-mL Source 15Q column (10 mM Tris pH 8.0 and 5 mM BME in a gradient of 0–400 mM NaCl developed over 40 mL), and finally dialyzed into 10 mM HEPES pH 7.0, 50 mM NaCl, 5% (w/v) glycerol, and 1 mM DTT for pull-down assays. Various SNX17-homologous C-terminal tails were purified using Glutathione Sepharose beads and directly dialyzed into 10 mM HEPES pH 7.0, 50 mM NaCl, 5% (w/v) glycerol, and 1 mM DTT for pull-down assays. Isolated MBP-tagged VPS26C was purified using Amylose beads (New England Biolabs) and eluted using 20 mM Tris pH 8.0, 200 mM NaCl, 2% (w/v) maltose, and 5 mM BME. The protein was further purified by anion exchange chromatography using a 2-mL Source 15S column (10 mM HEPES pH 7.0 and 5 mM BME in a gradient of 0–400 mM NaCl developed over 40 mL) and cleaved using TEV protease to remove the MBP tag. Cleaved VPS26C was polished by size exclusion chromatography using a 24-mL Superdex Increase 75 column [10 mM HEPES pH 7.0, 100 mM NaCl, 5% (w/v) glycerol, and 1 mM DTT]. MBP-CCDC22 VBD and MBP-CCDC93 VBD were purified as described[6]. All chromatography steps were performed using Cytiva columns on an ÄKTA™ Pure protein purification system. SNX17 C-terminal peptide, corresponding to amino acid sequence 451–470, ASASDVHGNFAFEGIGDEDL, was synthesized from GenScript at ≥98% purity. The lyophilized peptide was dissolved in 100 mM HEPES pH 7.0 buffer at a stock concentration of 40 mg/mL (19.5 mM), aliquoted in small volumes, and stored at −80 °C.

In vitro pull-down assays

GST pull-down experiments followed previous procedures[48]. Briefly, bait (100-200 pmol of GST-tagged proteins) and prey (50-200 pmol for Retriever) were mixed with 20 μL of Glutathione Sepharose beads (Cytiva) in 1 mL of binding buffer [10 mM HEPES pH 7, 50 mM NaCl, 5% (w/v) glycerol, 0.05% (w/v) Triton-X100, and 5 mM BME] at 4 °C for 30 min. After three 1-mL washes with the binding buffer, bound proteins were eluted with 100 mM Tris pH 8.5, 50 mM NaCl, and 30 mM reduced glutathione and examined by SDS-PAGE. Where it is indicated, 200 pmol of MBP-CCDC22-CCDC93 VBD dimer, various amounts of SNX17 CT peptide, various amounts of KRIT1 cargo peptide, or 200 nmol of PI(3)P diC4 (Echelon Biosciences) were added in pull-down assays. For mutagenesis pull-downs, VPS35L intensity was quantified and normalized to GST-CT intensity using ImageJ v2.3.0/1.53q. His6 pull-down assays were performed by mixing 50 pmol of His_6-tagged Retriever and 2000 pmol of SNX17 with 20 μL of TALON beads (Clontech Labs) in 1 mL of binding buffer [10 mM HEPES pH 7, 50 mM NaCl, 5% (w/v) glycerol, 0.05% (w/v) Triton-X100, and 5 mM BME] at 4 °C for 30 min. After three 1-mL washes with 20 mM Imidazole pH 7, 10 mM HEPES pH 7, 50 mM NaCl, 5% (w/v) glycerol, 0.05% (w/v) Triton-X100, and 5 mM BME, bound proteins were eluted with 200 mM Imidazole pH7, 10 mM HEPES pH 7, 50 mM NaCl, 5% (w/v) glycerol, and 5 mM BME and examined by SDS-PAGE. Where it is indicated, 6000 pmol of SNX17 CT peptide, or 200 nmol of PI(3)P diC4 were added in pull-down assays.

In vitro equilibrium pull-down (EPD) assays

Equilibrium pull-down assays were performed as previously described[48]. Briefly, 60 μL of Glutathione Sepharose beads (50% slurry equilibrated in a pull-down buffer [10 mM HEPES pH 7, 50 mM NaCl, 5% (w/v) glycerol, 0.05% (w/v) Triton-X100, and 5 mM BME] were mixed with 0.1 μM Retriever and various amounts of GST-tagged protein (up to 45 μM, stored in the same pull-down buffer) and brought to 100 μL final reaction volume using the pull-down buffer. The reactions were allowed to mix for 30 min at 4 °C, and four reactions at a time were spun at 15 krpm for 15 seconds. The supernatant was immediately removed and examined by SDS-PAGE and Coomassie blue staining. The VPS35L intensity was quantified using ImageJ v2.3.0/1.53q to calculate the fractional occupancy. The data from all repeats were pooled and globally fitted in DynaFit v4.08.187 using a single binding site model[49,50].

Sample preparation for electron microscopy

Purified Retriever and synthesized SNX17 CT peptide were mixed freshly at a final concentration of 1.4 μM Retriever and 6.5 mM peptide in a final buffer containing 10 mM HEPES pH 7.0, 150 mM NaCl, 5% (w/v) glycerol, and 1 mM DTT. The mixture was centrifuged for at least 10 min at 4 °C before 3 μL was applied to a glow-discharged Quantifoil 300-mesh R1.2/1.3 Copper grid (Micro Tools GmbH). After a 10-second preincubation under 100% humidity at 4 °C, the grid was blotted for 3.5 sec and plunge-frozen in liquid ethane using Vitrobot Mark IV (Thermo Fisher).

Electron microscopy data acquisition

Sample grids were screened on a 200 kV Talos Artica or Glacios microscope (Thermo Fisher) at the Cryo Electron Microscopy Facility by Structural Biology Laboratory at University of Texas Southwestern Medical Center (UTSW) or at the cryo-EM Facility at Iowa State University. The final cryo-EM data were acquired on a Titan Krios microscope (Thermo Fisher) at PNCC operated at 300 kV, with a post-column energy filter (Gatan) and a K3 direct detection camera (Gatan) in non-CDS mode. Movies were acquired using SerialEM v4.0[51] at a pixel size of 0.4133 Å in super-resolution counting mode, with an accumulated total dose of 60 $e^-/Å^2$ over 60 frames. The defocus range of the images was set between −0.9 to −2.5 µm. In total, 10,009 movies were collected for data processing.

Electron microscopy data processing

Cryo-EM data were processed using cryoSPARC[52] v4.4.1. Pre-processing was performed in cryoSPARC Live, including motion correction with a binning factor of 2, resulting in a pixel size of 0.8266 Å/pixel and Contrast Transfer Function (CTF) estimation. Blob picking was used in cryoSPARC Live and 1,009,886 particles were selected after initial 2D classification. After extensive 2D classification, 559,719 particles were selected for ab initio 3D reconstruction and heterogeneous refinement (Supplementary Fig. 2). The best resolved 3D class, containing 227,973 particles, underwent global and local CTF-refinement and a final non-uniform refinement, producing a full map with an overall resolution of 3.4 Å with a binned pixel size of 1.03 Å/pixel (deposited in EMD-43873 with its associated half maps). To improve the map quality on both ends of the map, two masks were generated—one for VPS29-bound half of VPS35L, and another for VPS26C-bound half. Signals outside the masks were subtracted and local refinement of the two regions were performed independently. The resulted maps were deposited with their half maps at EMD-43871 and EMD-43870, respectively (Supplementary Fig. 2d–f). DeepEMhancer v20220530_cu11[33] was then used with the unfiltered half maps to generate sharpened maps of the two locally refined maps, respectively, and a composite of the two was generated in UCSF ChimeraX v1.7.1 by the vop maximum command[53]. This composite map (EMD-43872/PDB-9AU7) was used for modeling and shown in Fig. 3 and Supplementary Fig 3c, d. All reported resolutions followed the gold-standard Fourier shell correlation (FSC) using the 0.143 criterion[54].

Atomic model building

A model of the Retreiver-SNX17 complex predicted by AlphaFold Multimer v2.3.1 was used as the initial model[55] for model building. Model was first docked and fitted into the sharpened composite map using ISOLDE[56] in ChimeraX, followed by iterations of real-space refinement in Phenix v1.21[57] with reference model and secondary structure restraints and manual building in COOT v0.9.8.8[58,59]. Model geometries were assessed by MolProbity in Phenix[60] (http://molprobity.biochem.duke.edu/), and the PDB Validation server[61] (www.wwpdb.org). Figures were generated using PyMOL v2.5.4 or ChimeraX v1.7.1[62].

AlphaFold prediction and analysis

AlphaFold version 2.3.1 (https://github.com/deepmind/alphafold) was installed on local NVidia A100 80GB GPU computers at Iowa State University ResearchIT or High-Performance Computing for AlphaFold Multimer prediction using standard AlphaFold procedures[55,58] as previously described[6].

Reproducibility and statistical analysis

To assess statistical significance, one-way ANOVA with Dunnett's post-hoc test was applied to compare multiple groups with one control group, using Prism v9.5.1 (GraphPad). An error probability below 5% ($p < 0.05$; * in Figure panels) was considered to imply statistical significance. All imaging and co-precipitation experiments were performed in two to four independent iterations. All in vitro pull-down assays were performed at least twice, unless otherwise indicated. Large scale proteomics were performed once, with key results confirmed using other methods.

Reporting summary

Further information on research design is available in the Nature Portfolio Reporting Summary linked to this article.

Data availability

Cryo-EM maps and models have been deposited in the EMDB, with accession number EMD-43870, EMD-43871, EMD-43872, and EMD-43873, and PDB, with accession number 9AU7. AlphaFold Multimer-derived models are available in ModelArchive, with the accession code ma-swt4h [https://doi.org/10.5452/ma-swt4h]. Mass spectrometry data have been deposited at the MassIVE repository, with accession number MSV000095676 [https://doi.org/10.25345/C5M902F39] and MSV000094101 [https://doi.org/10.25345/C5BV7B635]. Source data are provided for all uncropped western blots, Coomassie-blue gels, and all quantitative datasets presented in this paper. All information required to reanalyze the data reported here is publicly available. Any additional data will be shared upon request. Source data are provided with this paper.

References

1. Seaman, M. N., McCaffery, J. M. & Emr, S. D. A membrane coat complex essential for endosome-to-Golgi retrograde transport in yeast. *J. Cell Biol.* **142**, 665–681 (1998).
2. Haft, C. R. et al. Human orthologs of yeast vacuolar protein sorting proteins Vps26, 29, and 35: assembly into multimeric complexes. *Mol. Biol. Cell* **11**, 4105–4116 (2000).
3. Edgar, A. J. & Polak, J. M. Human homologues of yeast vacuolar protein sorting 29 and 35. *Biochem. Biophys. Res. Commun.* **277**, 622–630 (2000).
4. McNally, K. E. et al. Retriever is a multiprotein complex for retromer-independent endosomal cargo recycling. *Nat. Cell Biol.* **19**, 1214–1225 (2017).
5. Healy, M. D. et al. Structure of the endosomal Commander complex linked to Ritscher-Schinzel syndrome. *Cell* **186**, 2219–2237.e29 (2023).
6. Boesch, D. J. et al. Structural organization of the retriever-CCC endosomal recycling complex. *Nat. Struct. Mol. Biol.* **31**, 910–924 (2023).
7. Laulumaa, S., Kumpula, E. P., Huiskonen, J. T. & Varjosalo, M. Structure and interactions of the endogenous human Commander complex. *Nat. Struct. Mol. Biol.* **31**, 925–938 (2024).
8. Singla, A. et al. Endosomal PI(3)P regulation by the COMMD/CCDC22/CCDC93 (CCC) complex controls membrane protein recycling. *Nat. Commun.* **10**, 4271 (2019).
9. Bartuzi, P. et al. CCC- and WASH-mediated endosomal sorting of LDLR is required for normal clearance of circulating LDL. *Nat. Commun.* **7**, 10961 (2016).
10. Steinberg, F. et al. A global analysis of SNX27-retromer assembly and cargo specificity reveals a function in glucose and metal ion transport. *Nat. Cell Biol.* **15**, 461–471 (2013).
11. Harrison, M. S. et al. A mechanism for retromer endosomal coat complex assembly with cargo. *Proc. Natl Acad. Sci. USA* **111**, 267–272 (2014).
12. Yong, X. et al. SNX27-FERM-SNX1 complex structure rationalizes divergent trafficking pathways by SNX17 and SNX27. *Proc. Natl Acad. Sci. USA* **118**, e2105510118 (2021).
13. Simonetti, B. et al. SNX27-Retromer directly binds ESCPE-1 to transfer cargo proteins during endosomal recycling. *PLoS Biol.* **20**, e3001601 (2022).

14. Fjorback, A. W. et al. Retromer binds the FANSHY sorting motif in SorLA to regulate amyloid precursor protein sorting and processing. *J. Neurosci.* **32**, 1467–1480 (2012).
15. Temkin, P. et al. SNX27 mediates retromer tubule entry and endosome-to-plasma membrane trafficking of signalling receptors. *Nat. Cell Biol.* **13**, 715–721 (2011).
16. Gomez, T. S. & Billadeau, D. D. A FAM21-containing WASH complex regulates retromer-dependent sorting. *Dev. Cell* **17**, 699–711 (2009).
17. Gomez, T. S., Gorman, J. A., de Narvajas, A. A., Koenig, A. O. & Billadeau, D. D. Trafficking defects in WASH-knockout fibroblasts originate from collapsed endosomal and lysosomal networks. *Mol. Biol. Cell* **23**, 3215–3228 (2012).
18. Jia, D., Gomez, T. S., Billadeau, D. D. & Rosen, M. K. Multiple repeat elements within the FAM21 tail link the WASH actin regulatory complex to the retromer. *Mol. Biol. Cell* **23**, 2352–2361 (2012).
19. Derivery, E. et al. The Arp2/3 activator WASH controls the fission of endosomes through a large multiprotein complex. *Dev. Cell* **17**, 712–723 (2009).
20. Wan, C. et al. Panorama of ancient metazoan macromolecular complexes. *Nature* **525**, 339–344 (2015).
21. Phillips-Krawczak, C. A. et al. COMMD1 is linked to the WASH complex and regulates endosomal trafficking of the copper transporter ATP7A. *Mol. Biol. Cell* **26**, 91–103 (2015).
22. Mallam, A. L. & Marcotte, E. M. Systems-wide Studies Uncover Commander, a Multiprotein Complex Essential to Human Development. *Cell Syst.* **4**, 483–494 (2017).
23. Hanley, S. E. & Cooper, K. F. Sorting Nexins in Protein Homeostasis. *Cells* **10**, 17 (2020).
24. Leneva, N., Kovtun, O., Morado, D. R., Briggs, J. A. G. & Owen, D. J. Architecture and mechanism of metazoan retromer:SNX3 tubular coat assembly. *Sci Adv* **7**, eabf8598 (2021).
25. Kovtun, O. et al. Structure of the membrane-assembled retromer coat determined by cryo-electron tomography. *Nature* **561**, 561–564 (2018).
26. Lucas, M. et al. Structural Mechanism for Cargo Recognition by the Retromer Complex. *Cell* **167**, 1623–1635.e14 (2016).
27. Simonetti, B. et al. Molecular identification of a BAR domain-containing coat complex for endosomal recycling of transmembrane proteins. *Nat. Cell Biol.* **21**, 1219–1233 (2019).
28. Yong, X. et al. Mechanism of cargo recognition by retromer-linked SNX-BAR proteins. *PLoS Biol.* **18**, e3000631 (2020).
29. Gallon, M. et al. A unique PDZ domain and arrestin-like fold interaction reveals mechanistic details of endocytic recycling by SNX27-retromer. *Proc. Natl Acad. Sci. USA* **111**, E3604–E3613 (2014).
30. Ghai, R. et al. Structural basis for endosomal trafficking of diverse transmembrane cargos by PX-FERM proteins. *Proc. Natl Acad. Sci. USA* **110**, E643–E652 (2013).
31. Stiegler, A. L., Zhang, R., Liu, W. & Boggon, T. J. Structural determinants for binding of sorting nexin 17 (SNX17) to the cytoplasmic adaptor protein Krev interaction trapped 1 (KRIT1). *J. Biol. Chem.* **289**, 25362–25373 (2014).
32. Abramson, J. et al. Accurate structure prediction of biomolecular interactions with AlphaFold 3. *Nature* **630**, 493–500 (2024).
33. Sanchez-Garcia, R. et al. DeepEMhancer: a deep learning solution for cryo-EM volume post-processing. *Commun. Biol.* **4**, 874 (2021).
34. Kendall, A. K., Chandra, M., Xie, B., Wan, W. & Jackson, L. P. Improved mammalian retromer cryo-EM structures reveal a new assembly interface. *J. Biol. Chem.* **298**, 102523 (2022).
35. Steinberg, F., Heesom, K. J., Bass, M. D. & Cullen, P. J. SNX17 protects integrins from degradation by sorting between lysosomal and recycling pathways. *J. Cell Biol.* **197**, 219–230 (2012).
36. Stockinger, W. et al. The PX-domain protein SNX17 interacts with members of the LDL receptor family and modulates endocytosis of the LDL receptor. *EMBO J.* **21**, 4259–4267 (2002).
37. Yong, X., Mao, L., Seaman, M. N. J. & Jia, D. An evolving understanding of sorting signals for endosomal retrieval. *iScience* **25**, 104254 (2022).
38. Butkovic, R. et al. Mechanism and regulation of cargo entry into the Commander endosomal recycling pathway. *Nat. Commun.* **15**, 7180 (2024).
39. Purushothaman, L. K. & Ungermann, C. Cargo induces retromer-mediated membrane remodeling on membranes. *Mol. Biol. Cell* **29**, 2709–2719 (2018).
40. Lopez-Robles, C. et al. Architecture of the ESCPE-1 membrane coat. *Nat. Struct. Mol. Biol.* **30**, 958–969 (2023).
41. Hornbeck, P. V. et al. PhosphoSitePlus, 2014: mutations, PTMs and recalibrations. *Nucleic Acids Res.* **43**, D512-20 (2015).
42. Schaffer, B. E. et al. Identification of AMPK Phosphorylation Sites Reveals a Network of Proteins Involved in Cell Invasion and Facilitates Large-Scale Substrate Prediction. *Cell Metab.* **22**, 907–921 (2015).
43. Healy, M. D. et al. Proteomic identification and structural basis for the interaction between sorting nexin SNX17 and PDLIM family proteins. *Structure* **30**, 1590–1602.e6 (2022).
44. Starokadomskyy, P. et al. CCDC22 deficiency in humans blunts activation of proinflammatory NF-kB signaling. *J. Clin. Invest* **123**, 2244–2256 (2013).
45. Osborne, D. G., Piotrowski, J. T., Dick, C. J., Zhang, J. S. & Billadeau, D. D. SNX17 affects T cell activation by regulating TCR and integrin recycling. *J. Immunol.* **194**, 4555–4566 (2015).
46. Li, H. et al. Endosomal sorting of Notch receptors through COMMD9 dependent pathways modulates Notch signaling. *J. Cell Biol.* **211**, 605–617 (2015).
47. Mao, X. et al. GCN5 is a required cofactor for a ubiquitin ligase that targets NF-kB/RelA. *Genes Dev.* **23**, 849–861 (2009).
48. Chen, B. et al. Rac1 GTPase activates the WAVE regulatory complex through two distinct binding sites. *Elife* **6** e29795 (2017).
49. Kuzmic, P. Program DYNAFIT for the analysis of enzyme kinetic data: application to HIV proteinase. *Anal. Biochem.* **237**, 260–273 (1996).
50. Kuzmic, P. DynaFit–a software package for enzymology. *Methods Enzymol.* **467**, 247–280 (2009).
51. Mastronarde, D. N. Automated electron microscope tomography using robust prediction of specimen movements. *J. Struct. Biol.* **152**, 36–51 (2005).
52. Punjani, A., Rubinstein, J. L., Fleet, D. J. & Brubaker, M. A. cryoSPARC: algorithms for rapid unsupervised cryo-EM structure determination. *Nat. Methods* **14**, 290–296 (2017).
53. Pettersen, E. F. et al. UCSF Chimera–a visualization system for exploratory research and analysis. *J. Comput Chem.* **25**, 1605–1612 (2004).
54. Henderson, R. et al. Outcome of the first electron microscopy validation task force meeting. *Structure* **20**, 205–214 (2012).
55. Evans, R. et al. Protein complex prediction with AlphaFold-Multimer. *BioRxiv* https://doi.org/10.1101/2021.10.04.463034 (2022).
56. Croll, T. I. ISOLDE: a physically realistic environment for model building into low-resolution electron-density maps. *Acta Crystallogr. D. Struct. Biol.* **74**, 519–530 (2018).
57. Liebschner, D. et al. Macromolecular structure determination using X-rays, neutrons and electrons: recent developments in Phenix. *Acta Crystallogr. D. Struct. Biol.* **75**, 861–877 (2019).
58. Jumper, J. et al. Highly accurate protein structure prediction with AlphaFold. *Nature* **596**, 583–589 (2021).
59. Emsley, P., Lohkamp, B., Scott, W. G. & Cowtan, K. Features and development of Coot. *Acta Crystallogr. D. Biol. Crystallogr* **66**, 486–501 (2010).
60. Chen, V. B. et al. MolProbity: all-atom structure validation for macromolecular crystallography. *Acta Crystallogr. D. Biol. Crystallogr.* **66**, 12–21 (2010).

61. Burley, S. K. et al. Protein Data Bank (PDB): The Single Global Macromolecular Structure Archive. *Methods Mol. Biol.* **1607**, 627–641 (2017).
62. Pettersen, E. F. et al. UCSF ChimeraX: Structure visualization for researchers, educators, and developers. *Protein Sci.* **30**, 70–82 (2021).
63. Ashkenazy, H. et al. ConSurf 2016: an improved methodology to estimate and visualize evolutionary conservation in macromolecules. *Nucleic Acids Res.* **44**, W344–W350 (2016).

Acknowledgements

GST-SNX17 FL construct was a gift from Titus Boggon at Yale University School of Medicine. We thank the Research IT at Iowa State University for hardware resources, installation of AlphaFold, and ongoing computational & diagnostic support. We also thank the Proteomics core and the Flow Cytometry core at UT Southwestern. Electron Microscopy data were collected in collaboration with the Structural Biology Laboratory using the Cryo Electron Microscopy Facility at UT Southwestern Medical Center (partially supported by grant RP220582 from the Cancer Prevention & Research Institute of Texas [CPRIT] for cryo-EM studies) and the Iowa State University Cryo-EM Facility (supported by the Roy J. Carver Structural Initiative). We also thank Omar Davulcu at the Pacific Northwest Cryo-EM Center (PNCC, supported by NIH grant U24GM129547) for his help with data collection performed at the PNCC at OHSU and accessed through EMSL (grid.436923.9), a DOE Office of Science User Facility sponsored by the Office of Biological and Environmental Research. Research was supported by funding from the National Institutes of Health (R35 GM128786 to B.C., R01 DK107733 to E.B. and D.D.B, and R01 DK133229, R01 DK119360 to E.E.T.), the Welch Foundation (I-1944 to X.B.), and the National Science Foundation (CDF 2047640 to B.C. and D.D.B.).

Author contributions

B.C. and E.B. conceived the project. E.B. oversaw cell biological and proteomic experiments performed by A.S. B.C. oversaw protein purification, biochemical experiments, and AlphaFold predictions performed by D.J.B. with the help from A.S.E., C.N., and D.A.K. Z.C. oversaw cryo-EM grid preparation, data collection, single particle reconstruction, and atomic-model building by B.C., Y.H., and H.Y.J.F. X.B. helped with cryo-EM data processing and supported cryo-EM grid preparation and screening performed by B.C. at UTSW. Es.B. and A.L. performed proteomic data analyses. P.J. supervised cryo-EM grid preparation and data collection performed by D.J.B. at Iowa State. D.D.B. helped with cellular experiments and data interpretation. R.S. and E.E.T. performed cellular experiments related to LRMDA. B.C., H.Y.J.F., Z.C., and D.J.B. analyzed structures. E.B. and B.C. drafted the manuscript and prepared the figures with assistance from all other authors.

Competing interests

The authors declare no competing interests.

Additional information

Supplementary information The online version contains supplementary material available at https://doi.org/10.1038/s41467-024-54583-6.

Correspondence and requests for materials should be addressed to Emre E. Turer, Ezra Burstein or Baoyu Chen.

Peer review information *Nature Communications* thanks Oleksiy Kovtun, Momo Sae-Lee and the other, anonymous, reviewer(s) for their contribution to the peer review of this work. A peer review file is available.